

Normalization of Hepatic Homeostasis in the *Npc1<sup>nmf164</sup>* Mouse Model of Niemann-Pick Type C Disease  
Treated with the Histone Deacetylase Inhibitor Vorinostat

Andrew B. Munkacsy\*<sup>§1,2</sup>, Natalie Hammond\*<sup>1</sup>, Remy T. Schneider<sup>1</sup>, Dinindu S. Senanayake<sup>1</sup>,  
Katsumi Higaki<sup>3</sup>, Kirill Lagutin<sup>4</sup>, Stephen J. Bloor<sup>4</sup>, Daniel S. Ory<sup>5</sup>, Robert A. Maue<sup>6</sup>, Fannie W.  
Chen<sup>7</sup>, Antonio Hernandez-Ono<sup>8</sup>, Nicole Dahlson<sup>9</sup>, Joyce J. Repa<sup>9</sup>, Henry N. Ginsberg<sup>8</sup>, Yiannis A.  
Ioannou<sup>7</sup> and Stephen L. Sturley<sup>§10</sup>

<sup>1</sup>School of Biological Sciences and <sup>2</sup>Centre for Biodiscovery, Victoria University of Wellington, Wellington, New Zealand 6012. <sup>3</sup>Division of Functional Genomics, Research Center for Bioscience and Technology, Tottori University, Yonago, Japan 683-8503. <sup>4</sup>Callaghan Innovation, Lower Hutt, New Zealand 5040. <sup>5</sup>Department of Medicine, Washington University School of Medicine, St. Louis, Missouri 63110. <sup>6</sup>Departments of Physiology and Neurobiology and of Biochemistry, Geisel School of Medicine at Dartmouth, Hanover, New Hampshire 03755. <sup>7</sup>Department of Genetics and Genomic Sciences, Mount Sinai School of Medicine, New York, New York 10029. <sup>9</sup>Departments of Physiology and Internal Medicine, University of Texas Southwestern Medical Center, Dallas, Texas 75390, Departments of <sup>8</sup>Medicine, and <sup>10</sup>Genetics and Development, Columbia University Medical Center, New York, New York 10032.

<sup>§</sup> To whom correspondence should be addressed: A.B.M, School of Biological Sciences, Victoria University of Wellington, Alan MacDiarmid Building, Room 322, Wellington 6012, New Zealand. Tel.: 04-463-5171; Fax: 04-463-5331; Email: [andrew.munkacsy@vuw.ac.nz](mailto:andrew.munkacsy@vuw.ac.nz). S.L.S., Department of Genetics and Development, Columbia University Medical Center, 630 West 168<sup>th</sup> St., New York, New York 10032. Tel: 212-305-6304; Fax: 212-305-3079; Email: [sls37@columbia.edu](mailto:sls37@columbia.edu).

\* Co-first authors

**Keywords:** cholesterol, drug development, epigenetics, histone deacetylase (HDAC) inhibitor, lipid transport, lysosomal storage disease, neurodegenerative disease, sphingolipid, transcriptomics

## ABSTRACT

Niemann-Pick type C (NP-C) disease is a fatal genetic lipidosis for which there is no FDA-approved therapy. Vorinostat, an FDA-approved inhibitor of histone deacetylases, ameliorates lysosomal lipid accumulation in cultured NP-C patient fibroblasts. To assess the therapeutic potential of histone deacetylase inhibition, we pursued these *in vitro* observations in two murine models of NP-C disease. *Npc1<sup>nmf164</sup>* mice, which express a missense mutation in the NPC1 gene, were treated intraperitoneally, from weaning, with the maximum tolerated dose of Vorinostat (150 mg/kg, 5 days per week). Disease progression was measured via gene expression, liver function and pathology, serum and tissue lipid levels, body weight and lifespan. Transcriptome analyses of treated livers indicated multiple changes consistent with reversal of liver dysfunction that typifies NP-C disease. Significant improvements in liver pathology and function were achieved by this

treatment regimen; however, NPC1 protein maturation and levels, disease progression, weight loss, and animal morbidity were not detectably altered. Vorinostat concentrations were >200  $\mu$ M in the plasma compartment of treated animals, but were almost 100-fold lower in brain tissue. Apolipoprotein B metabolism and the expression of key components of lipid homeostasis in primary hepatocytes from null (*Npc1<sup>-/-</sup>*) and missense (*Npc1<sup>nmf164</sup>*) mutant mice were altered by Vorinostat treatment, consistent with a response by these cells independent of the status of the NPC1 locus. These results suggest that HDAC inhibitors have utility to treat visceral NP-C disease. However, it is clear that improved blood-brain barrier penetration will be required to alleviate the neurological symptoms of human NP-C disease.

## INTRODUCTION

Histone deacetylase (HDAC) inhibitors were initially identified as treatments for a variety of proliferative diseases, including T-cell lymphoma and other cancers (1). The mechanism of efficacy primarily reflects changes in the transcriptional program of rapidly growing cells, and in some cases results in altered expression of 2-10% of the genome (2,3). Subsequently, intervention at the histone acetylation/deacetylation axis of gene expression has been successfully applied to many unrelated diseases (4). Neurological disorders such as Alzheimer's disease, Huntington's disease, Parkinson's disease, amyotrophic lateral sclerosis and Friedrich's Ataxia have all been found to respond to HDAC inhibitors (4-6). The primary mechanism by which HDAC inhibitors influence these diseases remains undetermined and may well be multivariate. In some disorders (*e.g.*, cystic fibrosis), the treatment is associated with alterations at the proteostatic level due in part to activation of chaperone-mediated refolding pathways (7).

Niemann Pick type C (NP-C) disease is a rare lysosomal storage disorder typified by defective subcellular transport of cholesterol and sphingolipids as well as premature demise due to central nervous system (largely cerebellar) impairment (8). Autosomal recessive mutations in the NPC1 and NPC2 genes confer 95% and 5% of NP-C disease cases, respectively. Both genes are strikingly conserved throughout evolution (from yeast to humans), although their precise functions remain elusive (9,10). We have proposed that variation in the activity of additional genes influences NP-C disease severity, and these loci represent novel therapeutic interventions (11). To identify such NP-C disease modification pathways, we have used a model system-based approach in the yeast *Saccharomyces cerevisiae*. Our “*exacerbate-reverse*” strategy successfully identified 13 genetic loci whose individual absence conferred complete inviability to the yeast deletion of the NPC1 ortholog conditional upon sterol loading. This approach identified the status of histone acetylation as a key component of lipid accumulation in yeast and in cultured human fibroblasts that are deficient in the NP-C pathways (11). We and others have demonstrated that histone deacetylase inhibition by a variety of pharmacological agents normalizes lipid

homeostasis in rapidly growing immortalized cell lines derived from patients with NP-C disease (11-13). These studies have progressed to the extent that the FDA-approved HDAC inhibitor Vorinostat [suberoylanilide hydroxamic acid (SAHA), Zolinza®] is the focus of a clinical trial for safety and tolerability in adult NP-C patients (<https://clinicaltrials.gov/ct2/show/NCT02124083>).

Multi-tissue lipid accumulation and neurodegeneration define NP-C disease. The aberrant subcellular lipid storage is clearly associated with transcriptional dysregulation of numerous genes, including sterol regulatory element binding protein targets such as HMG-CoA reductase (HMGCR) and the low-density lipoprotein receptor (LDLR) (14,15). Any candidate intervention that can restore lipid homeostasis in cultured cells, however, must also be tested for an impact on NP-C disease pathology in an *in vivo* model. This is particularly critical given the challenge of predicting whether results in cell culture will be conserved in human trials (16). Here we describe the impact of Vorinostat in a murine model of NP-C disease caused by a missense mutation in the NPC1 gene. We show that this FDA-approved HDAC inhibitor normalizes hepatic transcriptional regulation of cholesterol, corrects apolipoprotein B homeostasis, and improves liver function and pathology, thus prompting the possibility that this intervention may treat visceral NP-C disease. With the regimens used here, however, there was no accompanying improvement in mortality or morbidity, likely due to the poor bioavailability of this drug to brain tissues. Overall, these studies establish HDAC inhibition as an attractive approach for treatment of NP-C disease while emphasizing the need for candidate inhibitors to overcome the blood-brain barrier.

## RESULTS

*Npc1 Missense Variants Can Be Refolded.* In the *Npc1<sup>nmf164</sup>* mouse, NP-C disease arises from an aspartic acid-to-glycine missense mutation at codon 1005 in NPC1 that resembles several NPC1 missense mutations that cause NP-C disease in humans (17). Specifically, the murine *Npc1<sup>D1005G</sup>* variant is contextually similar to the *Npc1<sup>S1004L</sup>*, *Npc1<sup>P1007A</sup>*, and *Npc1<sup>P1007L</sup>* variants associated with the juvenile form of human NP-C disease. The

*Npc1<sup>nmf164</sup>* mouse model presents with a less severe form of the disease than the *Npc1<sup>-/-</sup>* murine model but nevertheless exhibits an abbreviated lifespan, progressive weight loss, neurological impairment, and cellular lipid accumulation compared to control littermates (17).

In contrast to the *Npc1<sup>-/-</sup>* mutant mouse model, *Npc1<sup>nmf164</sup>* mice exhibit low but detectable levels of presumably functionally impaired NPC1 protein (17). To specifically determine whether this phenotype is due to misfolding and premature degradation of the *Npc1<sup>D1005G</sup>* variant, fibroblasts derived from the *Npc1<sup>nmf164</sup>* mouse were treated with glycerol, a chemical chaperone known to stabilize misfolded proteins (18). Glycerol increased expression levels of the *Npc1<sup>D1005G</sup>* protein compared to untreated cells (Fig. 1) and in addition promoted its maturation to a higher molecular weight form. The properties of the *Npc1<sup>D1005G</sup>* protein were then compared with *Npc1<sup>I1061T</sup>*, a previously described misfolded Npc1 variant associated with the most common form of human NP-C disease (18,19). NPC1-deficient human osteosarcoma U2OS cells expressing the *Npc1<sup>I1061T</sup>* protein were also treated with glycerol. Expression levels of the *Npc1<sup>I1061T</sup>* protein were also increased with glycerol treatment (Fig. 1), consistent with previous studies (18). To elucidate the possible contributions of lysosomal and proteasomal degradation to levels of the *Npc1<sup>D1005G</sup>* protein, the *Npc1<sup>nmf164</sup>* fibroblasts were treated with 3-methyladenine (3-MA, an autophagy inhibitor), and two inhibitors of the proteasome, MG132 and lactacystin. Each of these treatments increased expression and maturation of the *Npc1<sup>D1005G</sup>* protein (Fig. 1), implicating lysosomal and proteasomal pathways in the degradation of misfolded forms of the *Npc1<sup>D1005G</sup>* protein.

*Vorinostat Administration in a Misfolded Protein Mouse Model of NP-C Disease.* To investigate the role of Vorinostat as an NP-C therapeutic *in vivo*, we first assessed toxicity of this HDAC inhibitor in the *Npc1<sup>nmf164</sup>* NP-C murine model following i.p.-administration in a vehicle of 45% PEG 400 + 10% DMSO (hereafter called PEG/DMSO). This protocol was used previously to deliver Vorinostat across the blood-brain barrier and inhibit the metastasis of triple-negative breast cancer to the brain (20). Twenty-one day old, asymptomatic *Npc1<sup>nmf164</sup>* homozygous

mutant and wild type (WT) mice were injected daily with 50, 100, 150 or 200 mg/kg Vorinostat for seven days. All mice were viable after seven days; however, we observed significant weight loss in mice treated with 200 mg/kg Vorinostat. This is in agreement with 200 mg/kg being toxic in control mice as well as in a mouse model of Huntington's disease (5). Using the maximum tolerated dose and treatment regimen, we determined whether HDAC inhibition with Vorinostat can impact NP-C disease progression. Control (WT) and *Npc1<sup>nmf164</sup>* mice were treated with 150 mg/kg/day Vorinostat or the PEG/DMSO vehicle, 5 times per week from P21, an age where lipid accumulation already exists in the liver and brain (17). Treatment continued until P60, at which point disease symptoms (*i.e.*, weight loss, motor function deficits) are detectable in untreated *Npc1<sup>nmf164</sup>* animals (17).

*Transcriptional Modulation in Response to Vorinostat.* The lysosomal sequestration of free cholesterol and other bioactive lipids in NPC1-deficient animals has striking and chronologically early consequences in terms of gene regulation. Multiple components of lipid homeostasis and inflammation are transcriptionally upregulated and this dysregulation is rapidly normalized by treatment with the lipid chelator, 2-hydroxypropyl- $\beta$ -cyclodextrin (14,15). To test whether these pathways respond to Vorinostat in the liver of *Npc1<sup>nmf164</sup>* mice as well as comprehensively explore the impact of Vorinostat on hepatic gene expression in these animals, we performed RNA-Seq analysis on RNA isolated from the livers of Vorinostat and vehicle-treated *Npc1<sup>nmf164</sup>* mice. The transcripts were mapped to the mouse mm10 genome assembly, normalized, and quantified. Approximately 16-18 million reads per sample were obtained. Expression levels of 14,516 genes were measured, a number comparable to the 14,326 genes previously measured in the murine liver transcriptome (21). Expression of 844 genes (5.9% of the transcriptome) was significantly regulated (>0.6 log-fold change,  $p < 0.05$ ) by Vorinostat treatment, and out of these 844 genes, 603 (71.4%) were upregulated and 241 (28.6%) were downregulated (Fig. 2a-b, Supplemental Table S1). These genes were classified within an extensive array of Gene Ontology processes (Fig. 2a). Notable cellular aspects and processes relevant to NP-C disease and HDAC inhibition

include lipid metabolism, inflammation, and histone-mediated gene expression (Fig. 2c).

Critically, the Vorinostat-responsive genes include those known to be modulated by HDAC inhibitors in previous studies. For example, the GATA-binding transcription factor GATA1, a hallmark Vorinostat responsive gene (2,3,22), was upregulated 3.6 log<sub>2</sub>-fold ( $p = 0.0001$ ) in Vorinostat-treated *Npc1<sup>nmf164</sup>* mice compared to PEG/DMSO-treated *Npc1<sup>nmf164</sup>* mice (Fig. 2c). As previously observed (23,24), early growth response-1 (EGR1) and amyloid beta precursor-like protein 1 (APLP1) were elevated 1.2 log<sub>2</sub>-fold ( $p = 5.67 \times 10^{-4}$ ) and 2.56 log<sub>2</sub>-fold ( $p = 1.95 \times 10^{-19}$ ), respectively, after Vorinostat treatment (Fig. 2c). The aryl hydrocarbon receptor nuclear translocator-like protein 1 (ARNTL, also referred to as BMAL1), is repressed by HDAC3 (25) and was elevated 2.59 log<sub>2</sub>-fold ( $p = 1.18 \times 10^{-7}$ ) after treatment with Vorinostat (Fig. 2c). Likewise, we determined that Vorinostat reduced levels of the minichromosome maintenance protein-2 MCM2 by 0.67 log<sub>2</sub>-fold ( $p = 0.0015$ ) and the TATA-box binding protein TAF6L by 0.56 log<sub>2</sub>-fold ( $p = 0.004$ ) compared to PEG/DMSO-treated mice (Fig. 2c), consistent with the previously observed downregulation of these genes by HDAC inhibitors (26,27). Additionally, the cyclin D1 (CCND1) gene has been shown to decrease in expression by HDAC inhibition (28); here Vorinostat reduced CCND1 expression 1.34 log<sub>2</sub>-fold ( $p = 1.8 \times 10^{-6}$ ) (Fig. 2c). It is clear from these responses that a variety of HDAC isoforms, and thus their transcriptional targets, were affected by the treatment protocol in place, as would be anticipated for the impact of a global HDAC inhibitor like Vorinostat.

To determine the therapeutic potential of Vorinostat, we investigated the overlap of Vorinostat-mediated gene expression and candidate biomarkers previously shown to be transcriptionally dysregulated in NP-C disease. LYZ1 (Lysozyme 1) transcript levels are upregulated in the liver and brain of the *Npc1<sup>-/-</sup>* mouse (29), and plasma lysozyme activity is increased in the *Npc1<sup>-/-</sup>* mouse (30). Vorinostat treatment reduced hepatic expression of LYZ1 by 1.1 log<sub>2</sub>-fold ( $p = 4.37 \times 10^{-4}$ ) in *Npc1<sup>nmf164</sup>* mice compared to vehicle control (Fig. 2c). Likewise, the sterol regulatory element binding factor (SREBF1) is a transcription factor that regulates

cholesterol synthesis and is upregulated in NPC1-deficient hepatocytes (31), and SREBF1 expression was reduced with the Vorinostat treatment 0.64 log<sub>2</sub>-fold ( $p = 0.02$ ) compared to vehicle-treated *Npc1<sup>nmf164</sup>* mice (Fig. 2c). In addition, the oxysterol binding protein OSBPL3 and the perilipin PLIN4 were upregulated in independent studies of the liver of the *Npc1<sup>-/-</sup>* mouse (29,32), and we show here that the Vorinostat treatment reduced expression of OSBPL3 and PLIN4 by 1.4 log<sub>2</sub>-fold ( $p = 2.86 \times 10^{-7}$ ) and 1.3 log<sub>2</sub>-fold ( $p = 1.44 \times 10^{-5}$ ), respectively, in *Npc1<sup>nmf164</sup>* mice (Fig. 2c).

Similarly, several transcriptional pathways associated with inflammation (a characteristic of chronic NP-C disease) were normalized by treatment of the *Npc1<sup>nmf164</sup>* mouse with Vorinostat. For example, expression levels of four genes [metalloproteinase matrix-15 (MMP15), CD276 antigen (CD276), and histocompatibility antigens H2-Ab1 and H2-Eb1) that were consistently shown to be upregulated in *Npc1<sup>-/-</sup>* mice (29,32) were downregulated in Vorinostat-treated *Npc1<sup>nmf164</sup>* mice compared to vehicle-treated *Npc1<sup>nmf164</sup>* mice (Fig. 2c). Expression levels of three additional pro-inflammatory CD antigen genes (CD8a, CD79b, CD74) were similarly reduced by Vorinostat (Fig. 2c). Two S100a genes (S100a8, S100a9) that are targets of NFκβ and critical components of the immune response to liver damage (33), were upregulated with Vorinostat treatment (Fig. 2c). The cathelicidin antimicrobial peptide gene (CAMP) is required for inflammatory response regulation; expression of CAMP was upregulated in two studies of the *Npc1<sup>-/-</sup>* mouse (29,32) and downregulated in the *Npc1<sup>nmf164</sup>* mice treated with Vorinostat. These results suggest that Vorinostat activates an anti-inflammatory response as a consequence of NP-C disease in the *Npc1<sup>nmf164</sup>* mouse.

*Transcriptional Modulation of Cholesterol Metabolism.* We used Web Gene Ontology Enrichment Analysis Tool Kit (34) to identify pathways statistically over-represented within the 844 Vorinostat-regulated genes in the liver transcriptome of *Npc1<sup>nmf164</sup>* mice. In addition to amino acid metabolism ( $p = 0.0323$ ), four pathways associated with an anti-inflammatory response were enriched: GPCRs Class A Rhodopsin-like ( $p = 0.0008$ ), GPCRs Non-odorant ( $p = 0.0026$ ), GPCRs peptide ( $p = 0.0323$ ),

chemokine signaling pathway ( $p = 0.0082$ ). Of particular relevance to NP-C disease, the enrichment analysis revealed that genes critical to the biosynthesis of cholesterol were downregulated ( $p = 0.0014$ ) (Fig. 2c). qRT-PCR analysis for seven key genes (HMGCS1, HMGCR, MVK, MVD, IDI1, LSS, CYP51) was conducted on sets of three randomly selected mice from the RNA-Seq analysis (Fig. 3a-g). Vehicle- and Vorinostat-treated WT mice were included to determine if Vorinostat regulates these cholesterol biosynthesis genes independently from the status of the NPC1 pathway.

Our analyses suggest that the cholesterol biosynthetic pathway is significantly upregulated in the *Npc1<sup>nmf164</sup>* model, presumably in response to the lysosomal accumulation of cholesterol in association with reduced free cholesterol in regulatory pools such as the ER. Indeed, expression levels of HMGCS1, HMGCR, MVK, MVD, IDI1, LSS and CYP51 were significantly upregulated in the mutant mice relative to WT (Fig. 3a-g), ranging from an increase of 2-fold to 5.1-fold. Impressively, Vorinostat treatment significantly decreased the expression of all seven genes towards WT levels, with fold change ranging from 1.6-fold to 2.8-fold. Moreover, these changes were only identified in *Npc1<sup>nmf164</sup>* mice; expression levels of these seven genes in WT mice were not affected by Vorinostat treatment. In addition, we measured expression of LDLR, a gene that is strongly upregulated in NP-C disease (14,15); LDLR was upregulated 1.9-fold in vehicle-treated *Npc1<sup>nmf164</sup>* compared to vehicle-treated WT mice ( $p = 0.014$ ), and downregulated 1.7-fold in Vorinostat-treated *Npc1<sup>nmf164</sup>* compared to vehicle-treated *Npc1<sup>nmf164</sup>* mice ( $p = 0.044$ ) (Fig. 3h). Collectively, these results have three major implications. First, cholesterol homeostatic genes are elevated in *Npc1<sup>nmf164</sup>* mice at P60. Second, Vorinostat does not regulate expression of cholesterol metabolism genes in WT mice. Third, and most importantly, upon treatment with Vorinostat, eight genes critical to cholesterol homeostasis and NP-C disease were downregulated to WT levels.

*Lipid Metabolism is Fundamental to the Vorinostat Interactome.* To identify the core genes in the Vorinostat interactome, we used Phenolyzer (35) to visualize gene-gene interactions, protein-protein interactions, and

transcriptional regulation among the 844 genes in the Vorinostat interactome (Fig. 2a). This analysis distinguished CYP27B1, HMGCR, PNPLA3, and CHKA as the core hubs in the Vorinostat interactome, each with more than 20 interactions within the interactome (Fig. 4). CYP27B1 encodes a member of the cytochrome P450 superfamily of enzymes that hydroxylates 25-hydroxyvitamin D3 and regulates the level of biologically active vitamin D derived from cholesterol. Interestingly, vitamin D deficiency is associated with toxic lipid accumulation in chronic liver disease (36). HMGCR encodes the rate-limiting enzyme in cholesterol biosynthesis that is consistently upregulated in NP-C disease (14,15), and we show here that Vorinostat treatment restores this dysregulation to normal levels (Fig. 3b). PNPLA3 encodes a patatin-like phospholipase that is a genetic risk factor for lipid-mediated liver disease wherein overexpression confers hepatic steatosis (37). CHKA encodes choline kinase alpha, one of two mammalian enzymes that catalyze the phosphorylation of choline to phosphocholine in the biosynthesis of the major membrane phospholipid, phosphatidylcholine (38). The hubs of the Vorinostat interactome are all associated with lipid metabolism: specifically, our identification of HMGCR as a mediator of Vorinostat-mediated downregulation of cholesterol biosynthesis as well as a key hub in the Vorinostat interactome indicates that regulation of cholesterol biosynthesis is fundamental to the impact of Vorinostat on NP-C disease.

*Vorinostat Improves Liver Health.* To determine if the transcriptional regulation of cholesterol metabolism by Vorinostat has functional consequences, we measured serum levels of alanine aminotransferase (ALT), an enzyme that is elevated in NP-C disease as a consequence of liver damage (39). Serum ALT levels were significantly higher (73.9%) in the PEG/DMSO-treated *Npc1<sup>nmf164</sup>* mice compared to PEG/DMSO-treated control mice. Vorinostat treatment significantly reduced serum ALT levels in *Npc1<sup>nmf164</sup>* mice by 25.7% (Fig. 5a). Furthermore, Vorinostat treatment significantly reduced serum total cholesterol in *Npc1<sup>nmf164</sup>* mice by 22%, independent of HDL cholesterol or triglyceride concentrations (Fig. 5b-d).

Thin section, hematoxylin/eosin (H/E) staining

of fixed liver tissue revealed the marked accumulation of lipid-laden cells in untreated *Npc1<sup>nmf164</sup>* mice at P60 (Fig. 5e), characteristic of lipid accumulation at this stage of the disease in this mouse model (17). Treatment of *Npc1<sup>nmf164</sup>* mice with Vorinostat convincingly and significantly reduced the prevalence of lipid-laden cells by 48.9% ( $p < 0.001$ ) and elevated the presence of healthy hepatocytes, relative to vehicle controls (Fig. 5e). Taken together, the transcriptional normalization of hepatic cholesterol homeostatic genes and the reductions in serum cholesterol and ALT levels (liver function) in conjunction with improved liver histopathology, indicate a marked recovery from visceral NP-C disease due to Vorinostat treatment.

To determine if the Vorinostat-mediated changes in liver health correlate with changes in total lipid accumulation *in vivo*, we quantified levels of free cholesterol, sphingomyelin, sphingosine, glucosylceramide and lactosylceramide using GC/MS and LC/MS. Each of these lipids are biochemical hallmarks of late-stage NP-C disease in the liver (8). As the status of these lipids has not been reported for the *Npc1<sup>nmf164</sup>* mouse at P60, we first determined that these lipids were significantly increased in vehicle-treated *Npc1<sup>nmf164</sup>* mice compared to vehicle-treated WT mice (Fig. 6a-e). In accordance with the *Npc1<sup>-/-</sup>* and *Npc1<sup>11061T</sup>* mouse models of NP-C disease (14,19,40), the *Npc1<sup>nmf164</sup>* mice exhibit increased levels of these lipids relative to WT mice (Fig. 6a-e). Vorinostat did not detectably alter lipid levels in WT or *Npc1<sup>nmf164</sup>* mice (Fig. 6a-e). To further investigate a hallmark lipid using an independent method, we assessed free cholesterol levels using fluorescent microscopy. Filipin, a fluorescent stain for unesterified cholesterol, is a key tool used in the diagnosis of NP-C patients (8). As expected, we observed increased filipin fluorescence in vehicle-treated *Npc1<sup>nmf164</sup>* mice compared to vehicle-treated WT mice (Fig. 6f-g). However, filipin fluorescence did not indicate any change in free cholesterol levels after Vorinostat treatment. These results indicate that Vorinostat did not detectably reduce lipid accumulation in the liver using this treatment regime from P21 to P60. Together, these results of reduced ALT levels, reduced number of lipid-laden cells, and increased number of healthy hepatocytes coincident with no

apparent reduction in total mass of unesterified cholesterol suggest that Vorinostat re-proportions lipids, a phenomenon that would be consistent with partitioning of unesterified cholesterol in Kupffer cells by cyclodextrin (41).

*Vorinostat Treatment Does Not Delay Weight Loss or Extend Lifespan.* To determine the effect of Vorinostat on the lifespan of the *Npc1<sup>nmf164</sup>* mice, we monitored the weight of Vorinostat- and PEG/DMSO-treated mice during an extended treatment period from P21 to P90 using the regimen described above (150 mg/kg/day Vorinostat in PEG/DMSO vehicle, 5 times per week). In agreement with our prior toxicity study, Vorinostat-treated WT mice continued to gain weight beyond 10 weeks (Fig. 7a) and were not neurologically impaired compared to vehicle-treated mice. Relative to vehicle-treated WT mice, vehicle-treated *Npc1<sup>nmf164</sup>* mice significantly lost weight between 10-13 weeks ( $p = 0.0002$ ), a result consistent with prior characterization of the *Npc1<sup>nmf164</sup>* mice (17). There was no delay in the weight loss of Vorinostat-treated *Npc1<sup>nmf164</sup>* mice at any point during the treatment (Fig. 7a); treated and untreated animals lost weight and exhibited ataxia to similar levels from 9-10 weeks until death. Therapies that have delayed weight loss have also extended lifespan (14,42), thus the absence of change with Vorinostat treatment would predict that this intervention protocol does not extend lifespan. Indeed, Vorinostat-treated *Npc1<sup>nmf164</sup>* mice survived  $94 \pm 7$  days ( $n = 8$ ), a time range that is not different than the  $94 \pm 4$  days ( $n = 5$ ) lifespan of untreated *Npc1<sup>nmf164</sup>* mice.

*Penetration of the Blood-Brain Barrier by Vorinostat.* Despite its beneficial effect on the liver, the lack of effect of Vorinostat treatment on weight and lifespan of the *Npc1<sup>nmf164</sup>* mouse suggests that the drug fails to reach a concentration in the brain required to reverse the overall impact of the disease. Previously, a concentration of 5-10  $\mu\text{M}$  of Vorinostat was described as sufficient to limit lipid accumulation in cultured NP-C patient fibroblasts (11-13). To determine the drug concentration achieved in the brain, we quantified Vorinostat in plasma and brain of treated *Npc1<sup>nmf164</sup>* mice at P21 (Fig. 7b). The levels of Vorinostat in the plasma at 0.5, 1, 2 and 4 hours after injection were 222.29, 17.39, 3.01 and 0.97  $\mu\text{M}$ . In marked contrast, the levels of Vorinostat in the brain in the same animals

were 3.16, 0.23, and 0.12  $\mu\text{M}$ , at 0.5, 1, and 2 hours after injection, respectively and were below the minimum detection level of the assay at 4 hours (Fig. 7c). These results indicate a half-life of Vorinostat that is less than 60 minutes. Our findings of rapid clearance and <5% brain penetration, compared to plasma, in *Npc1<sup>nmf164</sup>* mice are in accordance with observations in normal mice and in a murine model of Huntington's disease (43,44).

*Improved Liver Function is Independent of NPC1 Expression.* To investigate the mechanism by which Vorinostat reduced ALT levels, we measured NPC1 mRNA and protein levels to test the hypothesis that Vorinostat elevated expression of the *Npc1<sup>D1005G</sup>* variant in the *Npc1<sup>nmf164</sup>* mouse. To determine whether Vorinostat upregulated NPC1 mRNA expression, we measured mRNA levels of NPC1 by quantitative real time PCR (Fig. 8a). Expression of NPC1 was not affected in either genotype with Vorinostat treatment, although NPC1 mRNA expression was modestly elevated in vehicle-treated *Npc1<sup>nmf164</sup>* compared to vehicle-treated WT mice ( $p = 0.066$ ). Quantification of Western blot analysis of liver protein extracts from treated and untreated animals ( $n = 7$  each group) indicated that the vehicle-treated *Npc1<sup>nmf164</sup>* mouse expressed 19% of the amount of NPC1 expressed by vehicle-treated WT mice ( $p = 5.76 \times 10^{-7}$ , Fig. 8b-c), consistent with previous reports that the *Npc1<sup>nmf164</sup>* mouse expressed 10-15% of WT levels of NPC1 (17). However, our analysis indicated equivalent steady state levels of NPC1 protein in Vorinostat-treated liver and vehicle control-treated livers. The mRNA levels of NPC2 were 4.7-fold higher ( $p = 0.016$ ) in vehicle-treated *Npc1<sup>nmf164</sup>* compared to vehicle-treated WT mice, a result that has been previously reported for the *Npc1<sup>-/-</sup>* null mutant and the *Npc1<sup>pf/pf</sup>* missense mutant mouse models of NP-C disease (45,46). However, there was no significant change in expression of NPC2 in Vorinostat-treated *Npc1<sup>nmf164</sup>* compared to vehicle-treated *Npc1<sup>nmf164</sup>* mice (Fig. 8d). These results suggest that the improvements in lipid metabolism and liver function occur independently of the concentration of the *Npc1<sup>D1005G</sup>* protein and are not a consequence of Vorinostat regulating the NPC1/NPC2 pathways at protein or mRNA levels.

*Vorinostat Does Not Increase Maturation of the Npc1<sup>D1005G</sup> Protein.* To further understand the

lack of impact of Vorinostat on expression of the *Npc1<sup>D1005G</sup>* protein in the liver of *Npc1<sup>nmf164</sup>* mice, we investigated maturation of the *Npc1<sup>D1005G</sup>* protein in the secretory pathway via two glycosidase digestion assays that have been previously used to characterize the *Npc1<sup>I1061T</sup>* protein (18,19). First, we used Endoglycosidase H (Endo H), an enzyme that removes immature high-mannose N-linked glycans from proteins. Second, we used Peptide:N-glycosidase F (PNGase F), an enzyme that removes all N-linked glycan residues regardless of the glycan modification. In livers of vehicle-treated WT mice, the NPC1 protein is glycosidase-sensitive represented by a mature species at ~225 kDa that is reduced to two deglycosylated species at ~200 kDa and ~150 kDa in response to the Endo H and PNGase F treatments, respectively (Fig. 8e). These results indicate that the wild-type NPC1 protein is glycosylated in the ER and further matured in the Golgi. Conversely, the *Npc1<sup>D1005G</sup>* protein in both vehicle- and Vorinostat-treated *Npc1<sup>nmf164</sup>* mice is predominantly a single species at ~150 kDa in undigested, Endo H-, and PNGase F-treated samples, with similar electrophoretic mobility to PNGase F-treated WT protein (Fig. 8e). These results indicate that the majority of *Npc1<sup>D1005G</sup>* protein in livers of *Npc1<sup>nmf164</sup>* mice lacks glycosylation and does not exit the ER as a result of misfolding. This defect was not corrected by Vorinostat treatment.

*Vorinostat Normalizes Apolipoprotein B Metabolism in NPC1 Null and Missense Mutant Hepatocytes.* Inhibition of histone deacetylation results in differential expression of 2-10% of the genome (2,3). In disorders such as cystic fibrosis, the success of Vorinostat treatment was, at least in part, due to activation of chaperone-mediated refolding pathways (7). Thus far, our data suggest that Vorinostat is therapeutic via a mechanism that does not require functional NPC1 (Fig. 3; Fig. 8). To directly test whether residual levels of NPC1 protein impact the response to Vorinostat treatment we compared primary hepatocytes prepared from *Npc1<sup>nmf164</sup>* and *Npc1<sup>-/-</sup>* mice. In contrast to the *Npc1<sup>nmf164</sup>* mice that produces low levels of NPC1 protein, the *Npc1<sup>-/-</sup>* model expresses a null variant of the NPC1 gene arising from a transposon insertion at the 5' end of the gene (47). Metabolic labeling of primary hepatocytes with [<sup>35</sup>S]methionine followed by

immunoprecipitation was used to quantify newly synthesized and secreted isoforms of apolipoprotein B (apoB100 and apoB48). These proteins are major exporters of lipid from the liver (48). As described previously (31), the synthesis of apoB100 by hepatocytes derived from *Npc1*<sup>-/-</sup> mice was elevated in response to the lipid accumulation underlying NP-C disease. Similarly, secretion of newly synthesized apoB100 was dramatically increased (507.3%,  $p = 0.006$ ) and apoB48 was marginally increased (18.8%,  $p = 0.0007$ ) in *Npc1*<sup>-/-</sup> hepatocytes compared to control hepatocytes from WT littermates (Fig. 9a-c). Despite the absence of the NPC1 protein in these cell lines, the *ex vivo* treatment of 10  $\mu$ M Vorinostat strikingly reduced secretion of apoB100 by 76% ( $p = 0.01$ ) to control levels (Fig. 9a-c). Interestingly, secretion of apoB48 was slightly elevated in Vorinostat-treated *Npc1*<sup>-/-</sup> hepatocytes compared to vehicle-treated *Npc1*<sup>-/-</sup> hepatocytes (23.5%,  $p = 0.046$ ). ApoB metabolism was also aberrant in primary hepatocytes from *Npc1*<sup>nmf164</sup> mice expressing the *Npc1*<sup>D1005G</sup> missense allele. Unlike the null mutant hepatocytes, secretion levels of apoB100 and apoB48 were significantly reduced by 57.2% ( $p = 0.04$ ) and 69.6% ( $p = 0.002$ ), respectively, in vehicle-treated *Npc1*<sup>nmf164</sup> hepatocytes compared to vehicle-treated control hepatocytes (Fig. 9d-f). Similar to the response of *Npc1*<sup>-/-</sup> hepatocytes to Vorinostat, secretion of newly synthesized apoB48 levels in media was significantly increased (413.7%,  $p = 0.0008$ ) in Vorinostat-treated *Npc1*<sup>nmf164</sup> hepatocytes compared to vehicle-treated mutant cells (Fig. 9d-f). Clearly, Vorinostat modulated the homeostasis of apoB in both null *Npc1*<sup>-/-</sup> and missense *Npc1*<sup>nmf164</sup> hepatocytes, further demonstrating that the mechanism of action of this drug is independent of NPC1.

To further investigate the efficacy of Vorinostat in *Npc1*<sup>-/-</sup> and *Npc1*<sup>nmf164</sup> primary hepatocytes, we measured expression of several genes integral to lipid metabolism (NPC1, HMGCR, ABCG1, APOB) and the cellular response to misfolded proteins (CHOP). The expression of NPC1 was significantly increased by 91% ( $p = 0.016$ ) in vehicle-treated *Npc1*<sup>nmf164</sup> cells compared to vehicle-treated control hepatocytes, and Vorinostat did not impact these expression levels (Fig. 10a), results that are consistent with NPC1 gene expression in the liver of *Npc1*<sup>nmf164</sup>

mice compared to controls (Fig. 8a). As expected, expression of NPC1 was significantly reduced (81.4%,  $p = 0.009$ ) in vehicle-treated *Npc1*<sup>-/-</sup> compared to vehicle-treated WT hepatocytes, and interestingly, albeit likely not functional, this was significantly upregulated following treatment with Vorinostat (Fig. 10a). The expression of APOB was significantly reduced by 50.1% ( $p = 0.0009$ ) in *Npc1*<sup>nmf164</sup> hepatocytes compared to WT hepatocytes, and markedly elevated by Vorinostat treatment beyond control levels in both *Npc1*<sup>nmf164</sup> ( $p = 0.0007$ ) and *Npc1*<sup>-/-</sup> hepatocytes ( $p = 0.04$ ) (Fig. 10b). The transcription factor, CCAAT-enhancer-binding protein homologous protein (CHOP), an indicator of ER stress that has been associated with disrupted apoB metabolism (49), was significantly increased in *Npc1*<sup>nmf164</sup> hepatocytes (111.6%,  $p = 0.0006$ ) compared to WT hepatocytes (Fig. 10c). In contrast, the expression of CHOP was significantly reduced in *Npc1*<sup>-/-</sup> hepatocytes by 40.4% ( $p = 0.03$ ) compared to control hepatocytes. This dysregulation was reduced further in both mutant cell types by Vorinostat treatment (49.9%,  $p = 0.0003$  in *Npc1*<sup>-/-</sup> and 23.7%,  $p = 0.001$  in *Npc1*<sup>nmf164</sup> cells) (Fig. 10c). These results suggest that Vorinostat transcriptionally modulates gene expression in *Npc1*<sup>nmf164</sup> and *Npc1*<sup>-/-</sup> hepatocytes independently from the status of the NPC1 locus.

In certain instances, the transcriptional response to Vorinostat by primary hepatocytes was more striking in the presence of residual NPC1 protein (*i.e.*, in *Npc1*<sup>nmf164</sup> hepatocytes). Relative to controls, expression of HMGCR was significantly reduced by 47.5% ( $p = 0.004$ ) in *Npc1*<sup>nmf164</sup> and by 53.4% ( $p = 0.0003$ ) in *Npc1*<sup>-/-</sup> hepatocytes (Fig. 10d), consistent with previously reported levels of processed (nuclear) SREBP2 in *Npc1*<sup>-/-</sup> hepatocytes (31). Interestingly, Vorinostat significantly increased HMGCR expression to control levels only in *Npc1*<sup>nmf164</sup> hepatocytes (136.5%,  $p = 0.002$ ). Similarly, the expression of ABCG1 was significantly increased in *Npc1*<sup>nmf164</sup> and *Npc1*<sup>-/-</sup> hepatocytes by 769.7% ( $p = 3.3 \times 10^{-5}$ ) and 206.7% ( $p = 0.0003$ ), respectively, compared to control hepatocytes (Fig. 10e), results that are in agreement with the previous demonstration of increased expression of ABCG1, a transporter that regulates efflux to HDL, in *Npc1*<sup>-/-</sup> hepatocytes (50). Vorinostat treatment significantly increased ABCG1 expression but only in *Npc1*<sup>nmf164</sup>



hepatocytes (92.7%,  $p = 0.001$ ), a mechanism consistent with observations on the anti-atherogenic effects of HDAC inhibition (51).

## DISCUSSION

The identification of FDA-approved drugs to treat NP-C disease remains elusive; in nearly two decades of effort since the molecular isolation of the NPC1 gene (52), only 2-hydroxypropyl- $\beta$ -cyclodextrin, the excipient of a failed neurosteroid treatment (53), has progressed to a Phase 3 clinical trial. As an alternate strategy, we applied unbiased, genome-wide, genetic screens in yeast and identified histone acetylation as a negative modifier of the NP-C disease pathway (11). Subsequently, we and others translated this finding by demonstrating the efficacy of HDAC inhibitors to reduce lipid accumulation in NP-C patient fibroblasts (11-13). We hypothesized that this therapeutic effect would be conserved *in vivo* and that the pathway to regulatory approval of Vorinostat for this orphan disease would be relatively rapid and unencumbered. In the present study, we tested the impact of intraperitoneal injection of Vorinostat in the *Npc1<sup>nmf164</sup>* mouse model of NP-C disease. We carefully reviewed toxicity and administration of Vorinostat, and used a concentration and dosing regimen that was the maximum tolerated dose in this animal. This regimen exceeded that used to treat murine models of cancer (the equivalent of a human dose of 400 mg/day). We were successful in that Vorinostat treatment was therapeutic for visceral NP-C disease, as evidenced by normalized liver lipid homeostasis at the transcriptional level and marked improvement of liver pathology and function. However, aspects of disease progression such as morbidity, mortality and neurodegeneration were not impacted, due, at least in part, to ineffective brain penetration.

We interpret these findings as a very promising step towards applying HDAC inhibitors as therapeutics for this disease, however the manner by which HDAC inhibitors may act remains to be determined. HDAC inhibitors impact expression of the genome in a global fashion, with immense capacity to simultaneously alter numerous metabolic pathways. Indeed, our results show that Vorinostat altered the expression of approximately 6% of the liver transcriptome of *Npc1<sup>nmf164</sup>* mice, a result consistent with previous

reports of Vorinostat regulating 2-10% of the genome (2,3). Most notably, we detected transcriptional regulation of genes involved in cholesterol homeostasis that correlate with reversal of NP-C disease. The HMGCS1, HMGCR, MVK, MVD, IDI1, LSS, CYP51 and LDLR genes were repressed by Vorinostat only in the *Npc1<sup>nmf164</sup>* mice, reflecting the successful treatment of hepatic NP-C disease as well as a therapeutic mechanism that is independent of NPC1. Interestingly, HDAC inhibitors have also been shown to repress expression of cholesterol homeostatic genes in U18666A-treated SH-SY5Y human neuroblastoma cells (54). HDAC inhibitors can further impact expression of the genome by directing recovery of misfolded mutated proteins via the induction of chaperone pathways (7). In *Npc1<sup>nmf164</sup>* mice, the *Npc1<sup>D1005G</sup>* variant protein persisted as an unglycosylated species that could be chased through the secretion pathway into a fully glycosylated mature species either by a refolding agent such as glycerol, or by protection from degradation. However, our studies demonstrate that this is not the predominant mechanism by which Vorinostat impacts NP-C disease in these animals.

Despite the overall transcriptional responsiveness of the *Npc1<sup>nmf164</sup>* missense mutant mouse, the Vorinostat treatment protocol used here did not detectably alter hepatic expression of NPC1 at either mRNA or protein levels or in terms of its maturation through the secretion pathway. Moreover, when we compared apoB homeostasis in primary hepatocytes from both missense (*Npc1<sup>nmf164</sup>*) and null (*Npc1<sup>-/-</sup>*) mice, we concluded that Vorinostat normalized both genotypes, relative to their own age-, gender- and background-matched controls. Interestingly, apoB levels were significantly increased in *Npc1<sup>-/-</sup>* mice in the BALB/c background and significantly decreased in *Npc1<sup>nmf164</sup>* mice in the C57BL/6 background, differences that may be consequences of the strain background and/or the NPC1 mutation. There is precedence for the impact of mouse background in the context of NPC1 missense mutations (*e.g.*, different lipidomic profiles in *Npc1<sup>I1061T</sup>* mice in the BALB/c and C57BL/6 backgrounds (19). Similarly, there is precedence for varying effects of the ~300 disease-causing mutations in NPC1 on the clinical progression of NP-C disease (8,55-57). Regarding

the efficacy of Vorinostat, the extent of misfolding and feasibility of refolding will be critical to decipher for different mutations in NPC1. Our results suggest that Vorinostat would be therapeutic in the liver of all NP-C patients regardless of mutation since the mechanism underlying improvement was predominantly independent of NPC1 expression.

It is clear that the bioavailability and stability of Vorinostat represents a significant but we believe surmountable hurdle to further progress. We determined that i.p. administration and a PEG/DMSO vehicle results in Vorinostat levels at  $<5 \mu\text{M}$  in the brain, 30 minutes after injection, a result in stark contrast to the  $60 \mu\text{M}$  concentration in plasma at the same juncture. Concentrations of  $5 \mu\text{M}$  are necessary to reduce lipid accumulation with 24 hour treatment in cell culture (11-13). Given the 12 minute half-life of Vorinostat in rats and dogs (58) compared to the effectively infinite half-life in cell culture, it is plausible that  $>5 \mu\text{M}$  is necessary to reduce lipid accumulation in the murine brain. Interestingly, using the PEG/DMSO vehicle and the 150 mg/kg dose in this study, i.p.-administered Vorinostat reduced the tumor size in the brain of a mouse model of brain cancer (20), a result that was attributed to a disrupted blood-brain barrier in brain cancer models (44). It is widely accepted that the murine and feline models of NP-C disease do not have a compromised blood-brain barrier (59,60). The blood-brain barrier could be circumvented by a variety of strategies. Rescue of neurodegenerative symptoms in mouse models of Huntington's disease have been accomplished by dissolving Vorinostat in 2-hydroxypropyl- $\beta$ -cyclodextrin (5,43). This is interesting, for although 2-hydroxypropyl- $\beta$ -cyclodextrin is a compound not known to cross the blood-brain barrier, perhaps it improves blood-brain barrier penetration of Vorinostat in the Huntington's disease studies. Intriguingly, 2-hydroxypropyl- $\beta$ -cyclodextrin alone, when administered directly into the CNS, is itself a promising therapeutic to treat NP-C disease (14,42) and is currently being evaluated in a

## EXPERIMENTAL PROCEDURES

**Animals.** Animal husbandry and experiments were approved by the Columbia University and Victoria University Animal Ethics Committees. Animals were exposed to alternating 12 h periods

of dark and light, and were fed a standard diet, ad libitum, until dissection. *Npc1<sup>nmf164</sup>* mutant and wild type (WT) littermates (C57BL/6 background) were generated by crossing heterozygous *Npc1<sup>nmf164</sup>* males and females. NPC1 genotyping was conducted by restriction digests of PCR

clinical trial. Indeed, Alam and colleagues recently demonstrated a striking synergy (approximate 2-fold life extension, relative to 2-hydroxypropyl- $\beta$ -cyclodextrin monotherapy) when treating *Npc1<sup>nmf164</sup>* mice (in a BALB/c background) by combining high concentrations of Vorinostat with therapeutic doses of 2-hydroxypropyl- $\beta$ -cyclodextrin in a PEG/DMSO vehicle (61). Although the confounding effect of using already therapeutic doses of 2-hydroxypropyl- $\beta$ -cyclodextrin and possibly PEG/DMSO remains to be determined, it is apparent that the pharmacokinetics of Vorinostat can be improved.

In summary, NP-C disease is a fatal pediatric neurodegenerative disease due to lysosomal accumulation of cholesterol and sphingolipids. Currently, there is no effective FDA-approved therapy to treat NP-C disease. Here we have translated prior results in a yeast model of NP-C disease and NP-C patient fibroblasts (11) to the *Npc1<sup>nmf164</sup>* mouse model of NP-C disease, wherein we report that a marked improvement in liver function was accompanied by normalized expression of key hepatic homeostatic genes in Vorinostat-treated mice. With these data we provide proof-of-principle that HDAC inhibition has the potential to be therapeutic *in vivo* in an animal model of NP-C disease. Indeed, the potential of Vorinostat to ameliorate peripheral NPC disease in adults is currently the object of a Phase 1/2 clinical trial (<https://clinicaltrials.gov/ct2/show/NCT02124083>). Our results indicate that Vorinostat treatment limits the aberrant upregulation of cholesterol biosynthesis and uptake that arises from lysosomal sequestration of cholesterol in NP-C disease. Consequently, this markedly improves the visceral pathophysiology of this disease. With improved blood-brain barrier penetration, we propose that Vorinostat and other HDAC inhibitors may prove useful for treatment of the neurological aspects of NP-C disease.

of dark and light, and were fed a standard diet, ad libitum, until dissection. *Npc1<sup>nmf164</sup>* mutant and wild type (WT) littermates (C57BL/6 background) were generated by crossing heterozygous *Npc1<sup>nmf164</sup>* males and females. NPC1 genotyping was conducted by restriction digests of PCR

amplicons as described (17). Mice were i.p.-administered with Vorinostat (LC Laboratories) in 10% DMSO and 45% polyethylene glycol 400, as previously described (20), from P21 to P60 (for all *in vivo* experiments except body weight/lifespan experiment, which were continued to P90). Disease progression was monitored in terms of weekly weight gain from P21 to P90. For all experiments except the pharmacokinetic assay, *Npc1<sup>nmf164</sup>* mutant mice and WT mice were anesthetized 6 h after the last injection with an i.p.-administered injection of ketamine (100 mg/kg) and xylazine (10 mg/kg), serum was collected, and animals were transcardially perfused with 0.9% saline solution. Following perfusion, half of the cerebrum and liver were removed and immediately frozen at -80°C for genetic and biochemical analysis with the other half fixed in 4% paraformaldehyde for histological analysis.

**Primary Hepatocytes and Cell Culture.** Primary hepatocytes were isolated from age- and background-matched control, *Npc1<sup>nmf164</sup>* (C57BL/6 background), and *Npc1<sup>-/-</sup>* (BALB/c background, generously provided by X. Huang and S. Walkley) mice (62). Filtered, washed cells were plated into collagen-coated 6-well plates at a density of 500,000 viable cells/well in DMEM + 10% fetal bovine serum (FBS). Fibroblasts derived from *Npc1<sup>nmf164</sup>* mutant mice and wild-type littermates or NPC1-deficient human osteosarcoma U2OS cells expressing the *Npc1<sup>11061T</sup>* protein, were generated and maintained as previously described (63).

**ApoB Metabolism.** For steady-state apoB labeling and immunoprecipitation, primary hepatocytes were incubated in methionine-free DMEM for 1 h, and then labeled with [<sup>35</sup>S]methionine in methionine-free DMEM for 2 h (64). Cells were collected in 200 µl of lysis buffer (62.5 mM sucrose, 0.5% sodium deoxycholate, 0.5% Triton X-100, 50 mM Tris-HCl, pH 7.4, 150 mM NaCl, 1 mM benzamidine, 5 mM EDTA, 100 U/ml aprotinin, 50 µg/ml leupeptin, 50 µg/ml pepstatin A, and 10 mM HEPES, pH 8.0) and boiled with sample buffer for 5 min. Trichloroacetic acid total precipitable <sup>35</sup>S counts of the cell lysate were determined and equal radiolabeled intracellular and medium protein was processed by immunoprecipitation (anti-lipoprotein B, Calbiochem) and separated on 4%

SDS-PAGE gels. The gels were dried under vacuum at 65°C for 2 h and exposed to x-ray films to visualize apoB100 and apoB48.

**RNA-Seq Analysis.** Total RNA was extracted from livers of *Npc1<sup>nmf164</sup>* vehicle control and Vorinostat-treated mice (7 animals per group) using PureLink RNA Mini Kit (Life Technologies) and processed for RNA-Seq analyses at the Australian Genome Research Facility. RNA-Seq libraries were prepared using TruSeq RNA v2 Kit (Illumina) and quantified using Bioanalyzer (Agilent). The prepared libraries were sequenced using an Illumina HiSeq 2000 (100 bp single end reads). The reads were mapped to the *Mus musculus* genome (Build version mm10) using TopHat (v2.0.13). Transcripts were assembled utilizing reference-based annotation with Cufflinks (v2.2.1). Gene expression was normalized and quantified using Trimmed Mean of M (TMM) values. Differential Gene Expression analysis of Vorinostat-treated mice relative to vehicle-treated mice was calculated using log<sub>2</sub> ratio (fold change) and statistically evaluated using edgeR. The dataset has been deposited at the NCBI GEO database. Gene Ontology processes of differentially expressed genes were classified using Protein ANalysis Through Evolutionary Relationships (PANTHER) and Mouse Genome Database (MGD) (65,66). WEB-based Gene Set ANalysis Toolkit (34) was used to conduct enrichment analyses of functions and pathways. Phenolyzer (35) was used to identify core components of the Vorinostat interactome.

**Reverse Transcription-Polymerase Chain Reaction.** Gene expression was measured using quantitative reverse transcription polymerase chain reaction (qRT-PCR). For validation of RNA-Seq results, 80 ng of total RNA was converted to mRNA using Power SYBR Green RNA-to-CT Kit (Applied Biosystems) and quantified using SYBR-green chemistry and a CFX Connect Real-Time PCR Detection System (Bio-Rad). For characterization of primary hepatocytes, RNA was isolated from cells with Trizol (Invitrogen), and was used as template in qRT-PCR using an Applied Biosystems 7900HT sequence detection system. The mRNA levels were calculated by the 2<sup>-ΔCT</sup> method (67) using the following 5' to 3' primer sequences: ABCG1 (F: GCTGTGCGTTTTGTGCTGTT, R: TGCAGCTCCAATCAGTAGTCCTAA) (14);

APOB (F: CTGGGCTCCAGCATTCTA, R: TCACCAGTCATTTCTGCCTTTG) (68); CHOP (F: CACCACACCTGAAAGCAGAAC, R: GGTGAAAGGCAGGGACTCA) (69); CYCLO (F: TGGAGAGCACCAAGACAGACA, R: TGCCGGAGTCGACAATGAT) (70); CYP51 (F: CCTGGATGGAGGTTTTACCC, R: TCTCTCGATGGGCTCTATCC); GAPDH (F: TGGCGCTGTGTCTGTGT, R: TCGGGTCTGATTTCTGTTTCTTC) (29); HMGCR (F: CTTGTGGAATGCCTTGTGATTG, R: AGCCGAAGCAGCACATGAT) (14); HMGCS (F: GCCGTGAACTGGGTGCGAA, R: GCATATATAGCAATGTCTCCTGCAA) (14); IDII (F: AAAGCCGAGTTGGGAATACCC, R: ACCATCAGATTGGGCCTTGTA); LDLR (F: GAGGAACTGGCGGCTGAA, R: GTGCTGGATGGGGAGGTCT) (14); LSS (F: GCGGCTGTGCGATGCT, R: AGGTAGCGAACCCGCCA); MVD (F: CCGGTCAACATCGCAGTTATC, R: TTGTGGTCGTTTTTAGCTGGT); MVK (F: GGTGTGGTCGGAACCTCCC, R: CCTTGAGCGGGTTGGAGAC); NPC1 (F: AACCGTGACACTGCAGGACAT, R: CTCATAATGGTGCAGTTCTTGTGT) (46); and NPC2 (F: TGGCGCCTGTGTCTGTGT, R: TCGGGTCTGATTTCTGTTTCTTC) (46). Primers without references were designed using Primer-BLAST (71).

**Immunoblotting and Deglycosylation.** Frozen liver was homogenized in RIPA buffer with the addition of protease inhibitors (Roche) and centrifuged at 16,000 xg. Protein concentration was measured using the BCA Protein Assay (Bio-Rad). For deglycosylation, protein extracts were combined with Glycoprotein Denaturation Buffer (5% SDS, 0.4 M DTT), denatured at 65°C for 10 min, treated with either GlycoBuffer 3 (New England Biolabs) and 1000 U Endoglycosidase H (New England Biolabs) or GlycoBuffer 2 (New England Biolabs) with 1% NP-40 and 1000 U Peptide-N-Glycosidase F (New England Biolabs), and incubated at 37°C for 7 h. Protein was denatured at 4°C for 30 min, loaded onto a 7.5% Bis-Tris gel, subjected to electrophoresis, transferred onto 0.2 µm PVDF membranes using a semi-dry system (Bio-Rad), and incubated with NPC1 antibody (Abcam ab134113 or Abcam ab36983) or actin antibody (Sigma). Membranes were probed with goat anti-mouse or goat anti-

rabbit secondary antibodies (GE Healthcare), visualized using ECLplus (GE Healthcare) with a fluorescent image analyzer (Fuji FLA-5100), and quantified using densitometry software (ImageJ).

**NPC1 Protein Refolding.** Cells were incubated in the presence and absence of glycerol, 3-methyladenine (3-MA), MG132 or lactacystin for 20 h at 37°C, lysed in 100 mM sodium phosphate pH 7.5, 150 mM NaCl, 2 mM EDTA, 1% IGEPAL CA-630 for 15 min at 4°C, and centrifuged for 5 min at 14,000 rpm at 4°C. Total cell lysates were denatured at 70°C for 10 min, subjected to SDS-PAGE electrophoresis through a 3-8% Tris-Acetate pre-cast gel (Invitrogen), transferred to nitrocellulose membrane (Protran), and probed using primary antibodies against NPC1 (Abcam ab134113) or Hsp70 (Millipore) and a secondary HRP-conjugated rabbit IgG (GE Healthcare). Proteins were visualized by chemiluminescence using SuperSignal West Dura substrate (Thermo Scientific) on a FluorChemQ imager (ProteinSimple) using AlphaView software (Alpha Innotech).

**Pharmacokinetics.** Vorinostat (150 mg/kg) was administered as described above with one injection in *Npc1<sup>nmf164</sup>* mice. Plasma and brain were collected at 30, 60, 120, and 240 minutes after the injection. Vorinostat levels were measured using LC-MS/MS as previously described (43).

**Serum Analysis.** Serum measurements of alanine aminotransferase (ALT) total cholesterol, HDL cholesterol, LDL cholesterol and triglyceride were assessed at a commercial laboratory (New Zealand Veterinary Pathology) as part of a general metabolic profile.

**Histology.** Fixed liver tissue was paraffin-embedded, and 5µm sections were stained with hematoxylin/eosin (H/E) by the Columbia University Medical Center Molecular Pathology Core Facility. The prevalence of lipid-laden cells was expressed as a fraction of total cells per field and quantified using SlidePath Tissue Image Analysis (Leica Biosystems, version 2.0) software at 20x magnification.

**Lipids.** Homogenized frozen tissue (half liver lobe) was used to prepare lipids by a modified Bligh and Dyer extraction procedure (72). Free cholesterol, sphingomyelin, sphingosine, glucosylceramide, and lactosylceramide were measured using LC/MS as previously described

(73,74) modified for use with a Shimadzu 8040 LC/MS system, an APCI source with MRM detection, and a Waters Acquity BEH C18 1.7  $\mu$ m 2.1 x 150 mm column. Standards (Avanti Polar Lipids) were used for quantification and all

measurements were normalized to liver weight. Subcellular accumulation of free cholesterol in liver sections was visualized using fluorescence of filipin as previously described (42) and quantified using densitometry software (ImageJ).

### Acknowledgments

We thank the Ara Parseghian Medical Research Foundation (to SLS and JJR), Dana's Angels Research Trust (to SLS) and NIH (DK54320 to SLS; DK082712 to YAI; NS092653 to DSO; and HL55638 to HNG) in support of these studies. ABM was supported as a Peter Pentchev Research Fellow of the National Niemann-Pick Disease Foundation, a Senior Fellow in Biomedical Sciences of the Charles Revson Foundation, an NIH Postdoctoral Fellow in Arteriosclerosis (Grant T32 HL07343), and received support from the Victoria University of Wellington University Research Fund. KH was supported by a grant from Ministry of Education, Culture, Science, Sports and Technology of Japan (20790728). We are grateful for the support of Rodney Rothstein and Michael Shelanski in the final stages of this study.

### Conflict of interest

There are no conflicts to report.

### Author contributions

ABM, NH and SLS conceived, coordinated and conducted the study and wrote the paper. RTS and RAM contributed to the toxicity study and the development of the drug administration protocol used for *in vivo* experiments. FWC and YAI provided technical assistance to the experiment in Figure 1. DSS provided technical assistance and contributed to the preparation of the Figure 2. KL and SJB provided technical assistance for the experiment shown in Figures 6a-e. DSO designed, performed and analyzed the experiments shown in Figures 7c-d. KH performed the experiment shown in Figures 8e. AH-O and HNG provided technical assistance to the experiments in Figures 9 and 10. ND and JJR provided technical assistance to the experiment in Figure 10. All authors reviewed the results and approved the final version of the manuscript.

### REFERENCES

1. Dokmanovic, M., Clarke, C., and Marks, P. A. (2007) Histone deacetylase inhibitors: overview and perspectives. *Mol Cancer Res* **5**, 981-989
2. Richon, V. M., Sandhoff, T. W., Rifkind, R. A., and Marks, P. A. (2000) Histone deacetylase inhibitor selectively induces p21WAF1 expression and gene-associated histone acetylation. *Proc Natl Acad Sci U S A* **97**, 10014-10019
3. Mitsiades, C. S., Mitsiades, N. S., McMullan, C. J., Poulaki, V., Shringarpure, R., Hideshima, T., Akiyama, M., Chauhan, D., Munshi, N., Gu, X., Bailey, C., Joseph, M., Libermann, T. A., Richon, V. M., Marks, P. A., and Anderson, K. C. (2004) Transcriptional signature of histone deacetylase inhibition in multiple myeloma: biological and clinical implications. *Proc Natl Acad Sci U S A* **101**, 540-545
4. Falkenberg, K. J., and Johnstone, R. W. (2014) Histone deacetylases and their inhibitors in cancer, neurological diseases and immune disorders. *Nat Rev Drug Discov* **13**, 673-691
5. Hockly, E., Richon, V. M., Woodman, B., Smith, D. L., Zhou, X., Rosa, E., Sathasivam, K., Ghazi-Noori, S., Mahal, A., Lowden, P. A., Steffan, J. S., Marsh, J. L., Thompson, L. M., Lewis, C. M., Marks, P. A., and Bates, G. P. (2003) Suberoylanilide hydroxamic acid, a histone deacetylase inhibitor, ameliorates motor deficits in a mouse model of Huntington's disease. *Proc Natl Acad Sci U S A* **100**, 2041-2046
6. Herman, D., Jenssen, K., Burnett, R., Soragni, E., Perlman, S. L., and Gottesfeld, J. M. (2006) Histone deacetylase inhibitors reverse gene silencing in Friedreich's ataxia. *Nat Chem Biol* **2**, 551-558

7. Hutt, D. M., Herman, D., Rodrigues, A. P., Noel, S., Pilewski, J. M., Matteson, J., Hoch, B., Kellner, W., Kelly, J. W., Schmidt, A., Thomas, P. J., Matsumura, Y., Skach, W. R., Gentsch, M., Riordan, J. R., Sorscher, E. J., Okiyoneda, T., Yates, J. R., 3rd, Lukacs, G. L., Frizzell, R. A., Manning, G., Gottesfeld, J. M., and Balch, W. E. (2010) Reduced histone deacetylase 7 activity restores function to misfolded CFTR in cystic fibrosis. *Nat Chem Biol* **6**, 25-33
8. Vanier, M. T. (2010) Niemann-Pick disease type C. *Orphanet J Rare Dis* **5**, 16
9. Munkacsı, A. B., Porto, A. F., and Sturley, S. L. (2007) Niemann-Pick type C disease proteins: orphan transporters or membrane rheostats? *Future Lipidol.* **2**, 357-367
10. Lopez, M. E., and Scott, M. P. (2013) Genetic dissection of a cell-autonomous neurodegenerative disorder: lessons learned from mouse models of Niemann-Pick disease type C. *Dis Model Mech* **6**, 1089-1100
11. Munkacsı, A. B., Chen, F. W., Brinkman, M. A., Higaki, K., Gutierrez, G. D., Chaudhari, J., Layer, J. V., Tong, A., Bard, M., Boone, C., Ioannou, Y. A., and Sturley, S. L. (2011) An "exacerbate-reverse" strategy in yeast identifies histone deacetylase inhibition as a correction for cholesterol and sphingolipid transport defects in human Niemann-Pick type C disease. *J Biol Chem* **286**, 23842-23851
12. Pipalia, N. H., Cosner, C. C., Huang, A., Chatterjee, A., Bourbon, P., Farley, N., Helquist, P., Wiest, O., and Maxfield, F. R. (2011) Histone deacetylase inhibitor treatment dramatically reduces cholesterol accumulation in Niemann-Pick type C1 mutant human fibroblasts. *Proc Natl Acad Sci U S A* **108**, 5620-5625
13. Wehrmann, Z. T., Hulett, T. W., Huegel, K. L., Vaughan, K. T., Wiest, O., Helquist, P., and Goodson, H. (2012) Quantitative comparison of the efficacy of various compounds in lowering intracellular cholesterol levels in Niemann-Pick type C fibroblasts. *PLoS One* **7**, e48561
14. Liu, B., Turley, S. D., Burns, D. K., Miller, A. M., Repa, J. J., and Dietschy, J. M. (2009) Reversal of defective lysosomal transport in NPC disease ameliorates liver dysfunction and neurodegeneration in the npc1<sup>-/-</sup> mouse. *Proc Natl Acad Sci U S A* **106**, 2377-2382
15. Taylor, A. M., Liu, B., Mari, Y., Liu, B., and Repa, J. J. (2012) Cyclodextrin mediates rapid changes in lipid balance in Npc1<sup>-/-</sup> mice without carrying cholesterol through the bloodstream. *J Lipid Res* **53**, 2331-2342
16. Wienkers, L. C., and Heath, T. G. (2005) Predicting in vivo drug interactions from in vitro drug discovery data. *Nat Rev Drug Discov* **4**, 825-833
17. Maue, R. A., Burgess, R. W., Wang, B., Wooley, C. M., Seburn, K. L., Vanier, M. T., Rogers, M. A., Chang, C. C., Chang, T. Y., Harris, B. T., Graber, D. J., Penatti, C. A., Porter, D. M., Szwegold, B. S., Henderson, L. P., Totenhagen, J. W., Trouard, T. P., Borbon, I. A., and Erickson, R. P. (2012) A novel mouse model of Niemann-Pick type C disease carrying a D1005G-Npc1 mutation comparable to commonly observed human mutations. *Hum Mol Genet* **21**, 730-750
18. Gelsthorpe, M. E., Baumann, N., Millard, E., Gale, S. E., Langmade, S. J., Schaffer, J. E., and Ory, D. S. (2008) Niemann-Pick type C1 I1061T mutant encodes a functional protein that is selected for endoplasmic reticulum-associated degradation due to protein misfolding. *J Biol Chem* **283**, 8229-8236
19. Praggastis, M., Tortelli, B., Zhang, J., Fujiwara, H., Sidhu, R., Chacko, A., Chen, Z., Chung, C., Lieberman, A. P., Sikora, J., Davidson, C., Walkley, S. U., Pipalia, N. H., Maxfield, F. R., Schaffer, J. E., and Ory, D. S. (2015) A murine Niemann-Pick C1 I1061T knock-in model recapitulates the pathological features of the most prevalent human disease allele. *J Neurosci* **35**, 8091-8106
20. Palmieri, D., Lockman, P. R., Thomas, F. C., Hua, E., Herring, J., Hargrave, E., Johnson, M., Flores, N., Qian, Y., Vega-Valle, E., Taskar, K. S., Rudraraju, V., Mittapalli, R. K., Gaasch, J. A., Bohn, K. A., Thorsheim, H. R., Liewehr, D. J., Davis, S., Reilly, J. F., Walker, R., Bronder, J. L., Feigenbaum, L., Steinberg, S. M., Camphausen, K., Meltzer, P. S., Richon, V. M., Smith, Q. R.,

- and Steeg, P. S. (2009) Vorinostat inhibits brain metastatic colonization in a model of triple-negative breast cancer and induces DNA double-strand breaks. *Clin Cancer Res* **15**, 6148-6157
21. Yu, Y., Ping, J., Chen, H., Jiao, L., Zheng, S., Han, Z. G., Hao, P., and Huang, J. (2010) A comparative analysis of liver transcriptome suggests divergent liver function among human, mouse and rat. *Genomics* **96**, 281-289
  22. Marks, P. A., and Breslow, R. (2007) Dimethyl sulfoxide to vorinostat: development of this histone deacetylase inhibitor as an anticancer drug. *Nat Biotechnol* **25**, 84-90
  23. Su, L., Cheng, H., Sampaio, A. V., Nielsen, T. O., and Underhill, T. M. (2010) EGR1 reactivation by histone deacetylase inhibitors promotes synovial sarcoma cell death through the PTEN tumor suppressor. *Oncogene* **29**, 4352-4361
  24. Claerhout, S., Lim, J. Y., Choi, W., Park, Y. Y., Kim, K., Kim, S. B., Lee, J. S., Mills, G. B., and Cho, J. Y. (2011) Gene expression signature analysis identifies vorinostat as a candidate therapy for gastric cancer. *PLoS One* **6**, e24662
  25. Yin, L., and Lazar, M. A. (2005) The orphan nuclear receptor Rev-erb $\alpha$  recruits the N-CoR/histone deacetylase 3 corepressor to regulate the circadian Bmal1 gene. *Mol Endocrinol* **19**, 1452-1459
  26. Liu, Y., He, G., Wang, Y., Guan, X., Pang, X., and Zhang, B. (2013) MCM-2 is a therapeutic target of Trichostatin A in colon cancer cells. *Toxicol Lett* **221**, 23-30
  27. Halsall, J. A., Turan, N., Wiersma, M., and Turner, B. M. (2015) Cells adapt to the epigenomic disruption caused by histone deacetylase inhibitors through a coordinated, chromatin-mediated transcriptional response. *Epigenetics Chromatin* **8**, 29
  28. Stimson, L., and La Thangue, N. B. (2009) Biomarkers for predicting clinical responses to HDAC inhibitors. *Cancer Lett* **280**, 177-183
  29. Alam, M. S., Getz, M., Safeukui, I., Yi, S., Tamez, P., Shin, J., Velazquez, P., and Haldar, K. (2012) Genomic expression analyses reveal lysosomal, innate immunity proteins, as disease correlates in murine models of a lysosomal storage disorder. *PLoS One* **7**, e48273
  30. Alam, M. S., Getz, M., Yi, S., Kurkewich, J., Safeukui, I., and Haldar, K. (2014) Plasma signature of neurological disease in the monogenetic disorder Niemann-Pick Type C. *J Biol Chem* **289**, 8051-8066
  31. Kulinski, A., and Vance, J. E. (2007) Lipid homeostasis and lipoprotein secretion in Niemann-Pick C1-deficient hepatocytes. *J Biol Chem* **282**, 1627-1637
  32. Cluzeau, C. V., Watkins-Chow, D. E., Fu, R., Borate, B., Yanjanin, N., Dail, M. K., Davidson, C. D., Walkley, S. U., Ory, D. S., Wassif, C. A., Pavan, W. J., and Porter, F. D. (2012) Microarray expression analysis and identification of serum biomarkers for Niemann-Pick disease, type C1. *Hum Mol Genet* **21**, 3632-3646
  33. Nemeth, J., Stein, I., Haag, D., Riehl, A., Longrich, T., Horwitz, E., Breuhahn, K., Gebhardt, C., Schirmacher, P., Hahn, M., Ben-Neriah, Y., Pikarsky, E., Angel, P., and Hess, J. (2009) S100A8 and S100A9 are novel nuclear factor kappa B target genes during malignant progression of murine and human liver carcinogenesis. *Hepatology* **50**, 1251-1262
  34. Wang, J., Duncan, D., Shi, Z., and Zhang, B. (2013) WEB-based GEne SeT AnaLysis Toolkit (WebGestalt): update 2013. *Nucleic Acids Res* **41**, W77-83
  35. Yang, H., Robinson, P. N., and Wang, K. (2015) Phenolyzer: phenotype-based prioritization of candidate genes for human diseases. *Nat Methods* **12**, 841-843
  36. Han, Y. P., Kong, M., Zheng, S., Ren, Y., Zhu, L., Shi, H., and Duan, Z. (2013) Vitamin D in liver diseases: from mechanisms to clinical trials. *J Gastroenterol Hepatol* **28 Suppl 1**, 49-55
  37. Li, J. Z., Huang, Y., Karaman, R., Ivanova, P. T., Brown, H. A., Roddy, T., Castro-Perez, J., Cohen, J. C., and Hobbs, H. H. (2012) Chronic overexpression of PNPLA3I148M in mouse liver causes hepatic steatosis. *J Clin Invest* **122**, 4130-4144
  38. Vance, D. E., and Vance, J. E. (2009) Physiological consequences of disruption of mammalian phospholipid biosynthetic genes. *J Lipid Res* **50 Suppl**, S132-137

39. Sayre, N. L., Rimkunas, V. M., Graham, M. J., Crooke, R. M., and Liscum, L. (2010) Recovery from liver disease in a Niemann-Pick type C mouse model. *J Lipid Res* **51**, 2372-2383
40. Fan, M., Sidhu, R., Fujiwara, H., Tortelli, B., Zhang, J., Davidson, C., Walkley, S. U., Bagel, J. H., Vite, C., Yanjanin, N. M., Porter, F. D., Schaffer, J. E., and Ory, D. S. (2013) Identification of Niemann-Pick C1 disease biomarkers through sphingolipid profiling. *J Lipid Res* **54**, 2800-2814
41. Davidson, C. D., Fishman, Y. I., Puskas, I., Szeman, J., Sohajda, T., McCauliff, L. A., Sikora, J., Storch, J., Vanier, M. T., Szente, L., Walkley, S. U., and Dobrenis, K. (2016) Efficacy and ototoxicity of different cyclodextrins in Niemann-Pick C disease. *Ann Clin Transl Neurol* **3**, 366-380
42. Davidson, C. D., Ali, N. F., Micsenyi, M. C., Stephney, G., Renault, S., Dobrenis, K., Ory, D. S., Vanier, M. T., and Walkley, S. U. (2009) Chronic cyclodextrin treatment of murine Niemann-Pick C disease ameliorates neuronal cholesterol and glycosphingolipid storage and disease progression. *PLoS One* **4**, e6951
43. Mielcarek, M., Benn, C. L., Franklin, S. A., Smith, D. L., Woodman, B., Marks, P. A., and Bates, G. P. (2011) SAHA decreases HDAC 2 and 4 levels in vivo and improves molecular phenotypes in the R6/2 mouse model of Huntington's disease. *PLoS One* **6**, e27746
44. Hanson, J. E., La, H., Plise, E., Chen, Y. H., Ding, X., Hanania, T., Sabath, E. V., Alexandrov, V., Brunner, D., Leahy, E., Steiner, P., Liu, L., Scarce-Levie, K., and Zhou, Q. (2013) SAHA enhances synaptic function and plasticity in vitro but has limited brain availability in vivo and does not impact cognition. *PLoS One* **8**, e69964
45. Aqul, A., Liu, B., Ramirez, C. M., Pieper, A. A., Estill, S. J., Burns, D. K., Liu, B., Repa, J. J., Turley, S. D., and Dietschy, J. M. (2011) Unesterified cholesterol accumulation in late endosomes/lysosomes causes neurodegeneration and is prevented by driving cholesterol export from this compartment. *J Neurosci* **31**, 9404-9413
46. Xie, X., Brown, M. S., Shelton, J. M., Richardson, J. A., Goldstein, J. L., and Liang, G. (2011) Amino acid substitution in NPC1 that abolishes cholesterol binding reproduces phenotype of complete NPC1 deficiency in mice. *Proc Natl Acad Sci U S A* **108**, 15330-15335
47. Loftus, S. K., Morris, J. A., Carstea, E. D., Gu, J. Z., Cummings, C., Brown, A., Ellison, J., Ohno, K., Rosenfeld, M. A., Tagle, D. A., Pentchev, P. G., and Pavan, W. J. (1997) Murine model of Niemann-Pick C disease: mutation in a cholesterol homeostasis gene. *Science* **277**, 232-235
48. Ota, T., Gayet, C., and Ginsberg, H. N. (2008) Inhibition of apolipoprotein B100 secretion by lipid-induced hepatic endoplasmic reticulum stress in rodents. *J Clin Invest* **118**, 316-332
49. Conlon, D. M., Thomas, T., Fedotova, T., Hernandez-Ono, A., Di Paolo, G., Chan, R. B., Ruggles, K., Gibeley, S., Liu, J., and Ginsberg, H. N. (2016) Inhibition of apolipoprotein B synthesis stimulates endoplasmic reticulum autophagy that prevents steatosis. *J Clin Invest* **126**, 3852-3867
50. Wang, M. D., Franklin, V., Sundaram, M., Kiss, R. S., Ho, K., Gallant, M., and Marcel, Y. L. (2007) Differential regulation of ATP binding cassette protein A1 expression and ApoA-I lipidation by Niemann-Pick type C1 in murine hepatocytes and macrophages. *J Biol Chem* **282**, 22525-22533
51. Van den Bossche, J., Neele, A. E., Hoeksema, M. A., de Heij, F., Boshuizen, M. C., van der Velden, S., de Boer, V. C., Reedquist, K. A., and de Winther, M. P. (2014) Inhibiting epigenetic enzymes to improve atherogenic macrophage functions. *Biochem Biophys Res Commun* **455**, 396-402
52. Carstea, E. D., Morris, J. A., Coleman, K. G., Loftus, S. K., Zhang, D., Cummings, C., Gu, J., Rosenfeld, M. A., Pavan, W. J., Krizman, D. B., Nagle, J., Polymeropoulos, M. H., Sturley, S. L., Ioannou, Y. A., Higgins, M. E., Comly, M., Cooney, A., Brown, A., Kaneski, C. R., Blanchette-Mackie, E. J., Dwyer, N. K., Neufeld, E. B., Chang, T. Y., Liscum, L., Tagle, D. A., and et al. (1997) Niemann-Pick C1 disease gene: homology to mediators of cholesterol homeostasis. *Science* **277**, 228-231



53. Griffin, L. D., Gong, W., Verot, L., and Mellon, S. H. (2004) Niemann-Pick type C disease involves disrupted neurosteroidogenesis and responds to allopregnanolone. *Nat Med* **10**, 704-711
54. Nunes, M. J., Moutinho, M., Gama, M. J., Rodrigues, C. M., and Rodrigues, E. (2013) Histone deacetylase inhibition decreases cholesterol levels in neuronal cells by modulating key genes in cholesterol synthesis, uptake and efflux. *PLoS One* **8**, e53394
55. Garver, W. S., Francis, G. A., Jelinek, D., Shepherd, G., Flynn, J., Castro, G., Walsh Vockley, C., Coppock, D. L., Pettit, K. M., Heidenreich, R. A., and Meaney, F. J. (2007) The National Niemann-Pick C1 disease database: report of clinical features and health problems. *Am J Med Genet A* **143A**, 1204-1211
56. Runz, H., Dolle, D., Schlitter, A. M., and Zschocke, J. (2008) NPC-db, a Niemann-Pick type C disease gene variation database. *Hum Mutat* **29**, 345-350
57. Stampfer, M., Theiss, S., Amraoui, Y., Jiang, X., Keller, S., Ory, D. S., Mengel, E., Fischer, C., and Runz, H. (2013) Niemann-Pick disease type C clinical database: cognitive and coordination deficits are early disease indicators. *Orphanet J Rare Dis* **8**, 35
58. Sandhu, P., Andrews, P. A., Baker, M. P., Koeplinger, K. A., Soli, E. D., Miller, T., and Baillie, T. A. (2007) Disposition of vorinostat, a novel histone deacetylase inhibitor and anticancer agent, in preclinical species. *Drug Metab Lett* **1**, 153-161
59. Pontikis, C. C., Davidson, C. D., Walkley, S. U., Platt, F. M., and Begley, D. J. (2013) Cyclodextrin alleviates neuronal storage of cholesterol in Niemann-Pick C disease without evidence of detectable blood-brain barrier permeability. *J Inherit Metab Dis* **36**, 491-498
60. Vite, C. H., Bagel, J. H., Swain, G. P., Prociuk, M., Sikora, T. U., Stein, V. M., O'Donnell, P., Ruane, T., Ward, S., Crooks, A., Li, S., Mauldin, E., Stellar, S., De Meulder, M., Kao, M. L., Ory, D. S., Davidson, C., Vanier, M. T., and Walkley, S. U. (2015) Intracisternal cyclodextrin prevents cerebellar dysfunction and Purkinje cell death in feline Niemann-Pick type C1 disease. *Sci Transl Med* **7**, 276ra226
61. Alam, M. S., Getz, M., and Haldar, K. (2016) Chronic administration of an HDAC inhibitor treats both neurological and systemic Niemann-Pick type C disease in a mouse model. *Sci Transl Med* **8**, 326ra323
62. Smedsrod, B., and Pertoft, H. (1985) Preparation of pure hepatocytes and reticuloendothelial cells in high yield from a single rat liver by means of Percoll centrifugation and selective adherence. *J Leukoc Biol* **38**, 213-230
63. Chen, F. W., Gordon, R. E., and Ioannou, Y. A. (2005) NPC1 late endosomes contain elevated levels of non-esterified ('free') fatty acids and an abnormally glycosylated form of the NPC2 protein. *Biochem J* **390**, 549-561
64. Dixon, J. L., Furukawa, S. and Ginsberg, H. N. (1991) Lawn, R. M. (1989) Oleate stimulates secretion of apolipoprotein B-containing lipoproteins from Hep G2 cells by inhibiting early intracellular degradation of apolipoprotein B. *J Biol Chem* **266**, 5080-5086
65. Mi, H., Muruganujan, A., Casagrande, J. T., and Thomas, P. D. (2013) Large-scale gene function analysis with the PANTHER classification system. *Nat Protoc* **8**, 1551-1566
66. Eppig, J. T., Blake, J. A., Bult, C. J., Kadin, J. A., Richardson, J. E., and Mouse Genome Database, G. (2015) The Mouse Genome Database (MGD): facilitating mouse as a model for human biology and disease. *Nucleic Acids Res* **43**, D726-736
67. Schmittgen, T. D., and Livak, K. J. (2008) Analyzing real-time PCR data by the comparative CT method. *Nat Protoc* **3**, 1101-1108
68. Tian, J., Goldstein, J. L., and Brown, M. S. (2016) Insulin induction of SREBP-1c in rodent liver requires LXRalpha-C/EBPbeta complex. *Proc Natl Acad Sci U S A* **113**, 8182-8187
69. Chuang, J. C., Cha, J. Y., Garmey, J. C., Mirmira, R. G., and Repa, J. J. (2008) Research resource: nuclear hormone receptor expression in the endocrine pancreas. *Mol Endocrinol* **22**, 2353-2363

70. Cha, J. Y., and Repa, J. J. (2007) The liver X receptor (LXR) and hepatic lipogenesis. The carbohydrate-response element-binding protein is a target gene of LXR. *J Biol Chem* **282**, 743-751
71. Ye, J., Coulouris, G., Zaretskaya, I., Cutcutache, I., Rozen, S., and Madden, T. L. (2012) Primer-BLAST: a tool to design target-specific primers for polymerase chain reaction. *BMC Bioinformatics* **13**, 134
72. Bligh, E. G., and Dyer, W. J. (1959) (1959) A rapid method of total lipid extraction and purification. *Can J Biochem Physiol* **37**, 911-917
73. Butovich, I. A. (2009) Cholesteryl esters as a depot for very long chain fatty acids in human meibum. *J Lipid Res* **50**, 501-513
74. Shaner, R. L., Allegood, J. C., Park, H., Wang, E., Kelly, S., Haynes, C. A., Sullards, M. C., and Merrill, A. H., Jr. (2009) Quantitative analysis of sphingolipids for lipidomics using triple quadrupole and quadrupole linear ion trap mass spectrometers. *J Lipid Res* **50**, 1692-1707

**Abbreviations:** HDAC, histone deacetylase; NP-C, Niemann-Pick type C

## FIGURE LEGENDS

**Figure 1. Refolding of *Npc1*<sup>D1005G</sup> mutant protein.** Representative image of 30 µg of total cell lysates extracted from *Npc1*<sup>nmf164</sup> fibroblasts treated with 5% glycerol (Gly), 10 µM 3-methyladenine (3MA), 10 µM MG132 (MG), and 10 µM lactacystin (L) compared to U2OS cells expressing the *Npc1*<sup>I1061T</sup> mutation in the presence and absence of 5% glycerol. Lysates were denatured at 70°C for 10 min, electrophoresed through a 3-8% Tris-Acetate gel, and transferred onto a Protran membrane that was incubated with NPC1 or HSP70 antibody and envisaged with chemiluminescence.

**Figure 2. Vorinostat administration from P21 to P60 alters the liver transcriptome of *Npc1*<sup>nmf164</sup> mice.** a) Quantification of the diversity of biological processes regulated by Vorinostat as assigned using PANTHER (19). b) Heat map depicting the relative repression or induction of 844 transcripts that were differentially expressed in the liver by  $\geq 0.6$  log<sub>2</sub> ratio fold change ( $p < 0.05$ ) between the vehicle- and Vorinostat-treated *Npc1*<sup>nmf164</sup> mice (n = 7, both groups). c) Functional gene annotation clustering performed on 10 genes identified in cellular functions associated with inhibition of histone deacetylation, 19 genes with cellular functions associated with lipid metabolism, and 16 genes with cellular functions associated with inflammation. The scale bar indicates proportional read counts with red and white tones representing downregulated and upregulated genes, respectively; this scale bar applies to panels b and c.

**Figure 3. Vorinostat normalizes gene expression of key components of cholesterol homeostasis.** 80 ng of RNA from the indicated animals were assessed for gene expression at P60 using qRT-PCR relative to GAPDH (PCR primer are described in experimental procedures). Vehicle-treated WT mice were assigned a baseline expression of 1. a-g) Cholesterol biosynthesis genes that were significantly enriched in RNA-Seq analysis (HMGCS, HMGCR, MVK, MVD, IDI1, LSS, CYP51). h) Low-density lipoprotein receptor (LDLR). All groups are n = 3 with data shown as mean  $\pm$  S.D. \*,  $p < 0.05$ , Student's *t* test.

**Figure 4. Lipid metabolism is fundamental to the Vorinostat interactome.** The 844 genes in the Vorinostat interactome were processed through Phenolyzer (35) to visualize the 50 most interactive genes based on gene-gene interactions, protein-protein interactions, and transcriptional regulation within the interactome. This analysis distinguished four lipid metabolism genes (CYP27B1, HMGCR, PNPLA3, CHKA) as the core hubs (indicated in blue) in the Vorinostat interactome, each with more than 20 interactions within the interactome. Size of nodes represents number of interactions.

**Figure 5. Vorinostat treatment improves liver function in *Npc1*<sup>nmf164</sup> mice.** Animals were treated with either vehicle (PEG/DMSO) or 150 mg/kg Vorinostat from P21 to P60, at which point serum was harvested from sacrificed animals. Liver function was evaluated via levels of alanine aminotransferase (ALT) expressed as International Units/Liter (IU/L, panel a). Total cholesterol, HDL cholesterol, and triglycerides (panels b –d) were measured and are expressed as mmol/L. All data are shown as mean  $\pm$  S.E. WT + PEG/DMSO (n = 5); WT + Vorinostat (n = 5); *Npc1*<sup>nmf164</sup> + PEG/DMSO (n = 4); *Npc1*<sup>nmf164</sup> + Vorinostat (n = 5). \*,  $p < 0.05$ , Student's *t* test. e) Fixed liver tissue was paraffin-embedded and 5µm sections were stained with hematoxylin/eosin (H/E). Representative images are shown. The prevalence of lipid-laden cells was expressed as a fraction of total cells per field (approximately 3000) and quantified using SlidePath Tissue Image Analysis (Leica Biosystems, version 2.0) software at 20x magnification. Data are shown in panel (f) as mean  $\pm$  S.D. from 10-15 random fields per animal with 3 animals per treatment group. \*,  $p < 0.001$ , Student's *t* test. The inset panels represent an 80x magnification of the field of view, focusing on the lipid laden cells.

**Figure 6. Cholesterol and sphingolipid accumulation in the liver of Vorinostat treated mice.** WT and *Npc1*<sup>nmf164</sup> mice were treated with either vehicle (PEG/DMSO) or 150 mg/kg Vorinostat from P21 to P60, at which time livers were harvested from sacrificed animals. a-e) Free cholesterol and sphingolipids were measured using LC/MS. All groups are n = 5 with data shown as mean  $\pm$  S.D. \*,  $p < 0.05$ ,

Student's *t* test. f-g) Unesterified cholesterol was visualized using filipin and quantified using densitometry software (ImageJ). All groups are *n* = 3 with data shown as mean ± S.D. \*, *p* < 0.05, Student's *t* test.

**Figure 7. Vorinostat does not delay weight loss or penetrate the blood-brain barrier of *Npc1<sup>nmf164</sup>* mice.** a) Animals were treated with PEG/DMSO or 150 mg/kg Vorinostat between P21-P90 (3-13 weeks) and weighed weekly. Data are shown as mean ± S.D. WT + PEG/DMSO (*n* = 5); WT + PEG/DMSO (*n* = 5); *Npc1<sup>nmf164</sup>* + PEG/DMSO (*n* = 5); *Npc1<sup>nmf164</sup>* + Vorinostat (*n* = 6). \*, *p* < 0.05, two-way ANOVA with Bonferroni post-hoc test. b-c) Vorinostat levels in the brain are <5% of plasma levels. 150 mg/kg Vorinostat was administered in *Npc1<sup>nmf164</sup>* mice at P21, and mean Vorinostat levels were quantified in plasma and brain at three time points after injection (0.5, 1, 2 and 4 hours).

**Figure 8. Liver recovery due to Vorinostat treatment is independent of changes in expression of NPC1 or NPC2.** Animals were treated with either vehicle (PEG/DMSO) or 150 mg/kg Vorinostat from P21 to P60. a) Liver RNA from the indicated animals was assessed for NPC1 gene expression by qRT-PCR relative to GAPDH. All groups are *n* = 3 with data shown as mean ± S.D. b) Representative image of 30 µg of hepatic protein extracted from vehicle- and Vorinostat-treated animals that was denatured at 4°C for 30 min, subjected to electrophoresis, transferred onto PVDF membrane and incubated with NPC1 antibody or actin antibody. c) NPC1 and actin bands were quantified relative to actin using densitometry software (ImageJ). All groups are *n* = 7 with data shown as mean ± S.E. \*, *p* < 0.05, Student's *t* test. d) Liver RNA from the indicated animals was assessed for NPC2 gene expression by qRT-PCR relative to GAPDH. All groups are *n* = 3 with data shown as mean ± S.D. \*, *p* < 0.05, Student's *t* test. e) Protein from the indicated animals was extracted, treated with glycosidase enzymes, and analyzed via SDS-PAGE/immunoblotting and probed for NPC1 expression.

**Figure 9. Vorinostat modulates apoB metabolism in *Npc1<sup>nmf164</sup>* and *Npc1<sup>-/-</sup>* hepatocytes.** Hepatocytes were isolated from livers of *Npc1<sup>nmf164</sup>* and *Npc1<sup>-/-</sup>* mice, incubated for 24 hours in DMEM + 10% FBS with 10 µM Vorinostat or DMSO, and labeled with [<sup>35</sup>S]methionine in methionine-free DMEM for 2 h. Equal radiolabeled protein was separated on a 4% SDS-PAGE gel to distinguish apoB100 and apoB48 in mutant mice relative to appropriate WT controls. a-c) Newly synthesized and secreted apoB in media of *Npc1<sup>-/-</sup>* hepatocytes. d-f) Newly synthesized and secreted apoB in media of *Npc1<sup>nmf164</sup>* hepatocytes. Data represent mean cpm ± S.D. from triplicates. \*, *p* < 0.05, Student's *t* test.

**Figure 10. Transcriptional response of *Npc1<sup>nmf164</sup>* and *Npc1<sup>-/-</sup>* hepatocytes following treatment with Vorinostat.** Hepatocytes were isolated from livers of *Npc1<sup>nmf164</sup>* and *Npc1<sup>-/-</sup>* mice, incubated for 24 hours in DMEM + 10% FBS with 10 µM Vorinostat or DMSO, and assessed for NPC1, APOB, CHOP, HMGCR and ABCG1 gene expression by qRT-PCR relative to cyclophilin (CYCLO) and appropriate WT controls using primers described in Methods. All groups are *n* = 3 with data shown as mean ± S.D. \*, *p* < 0.05, Student's *t* test.

**Figure 1**

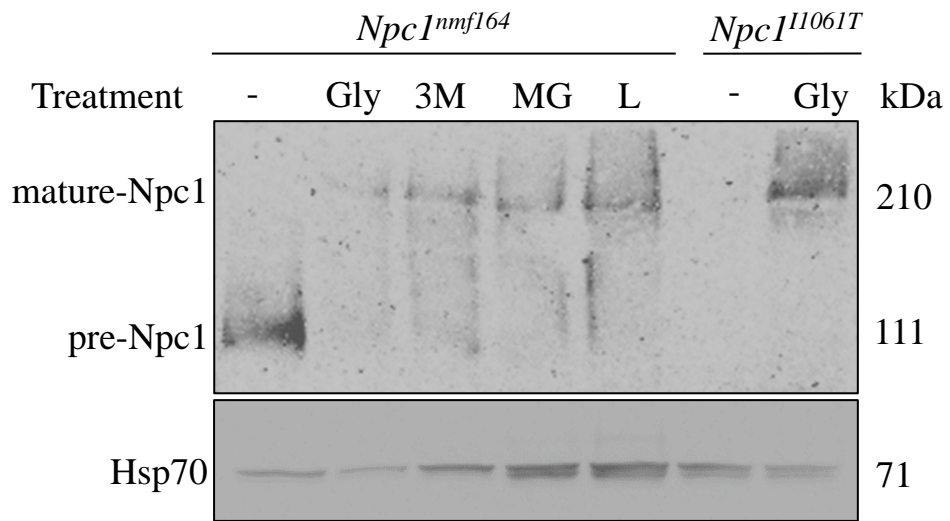


**Figure 2**

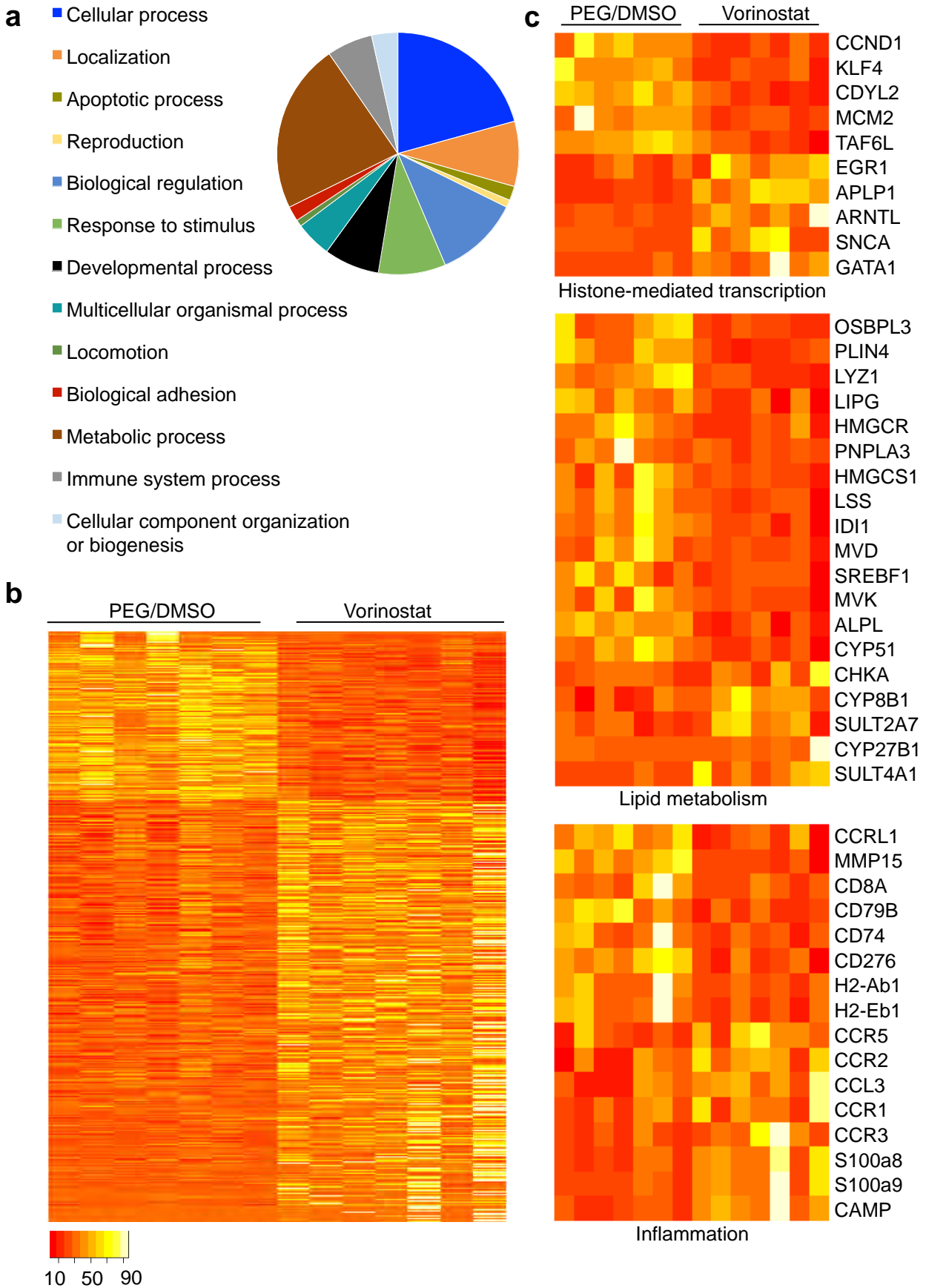


**Figure 3**

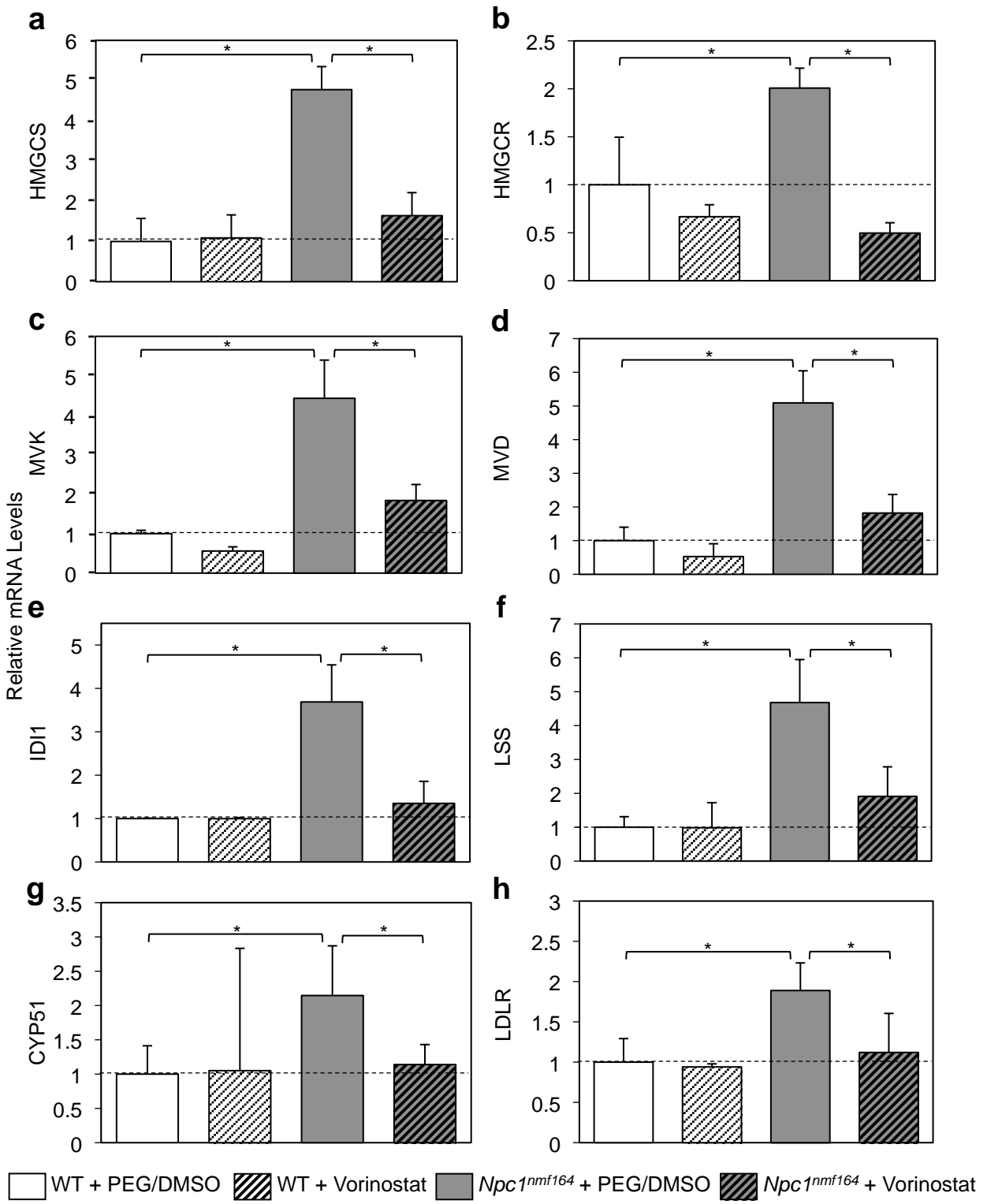
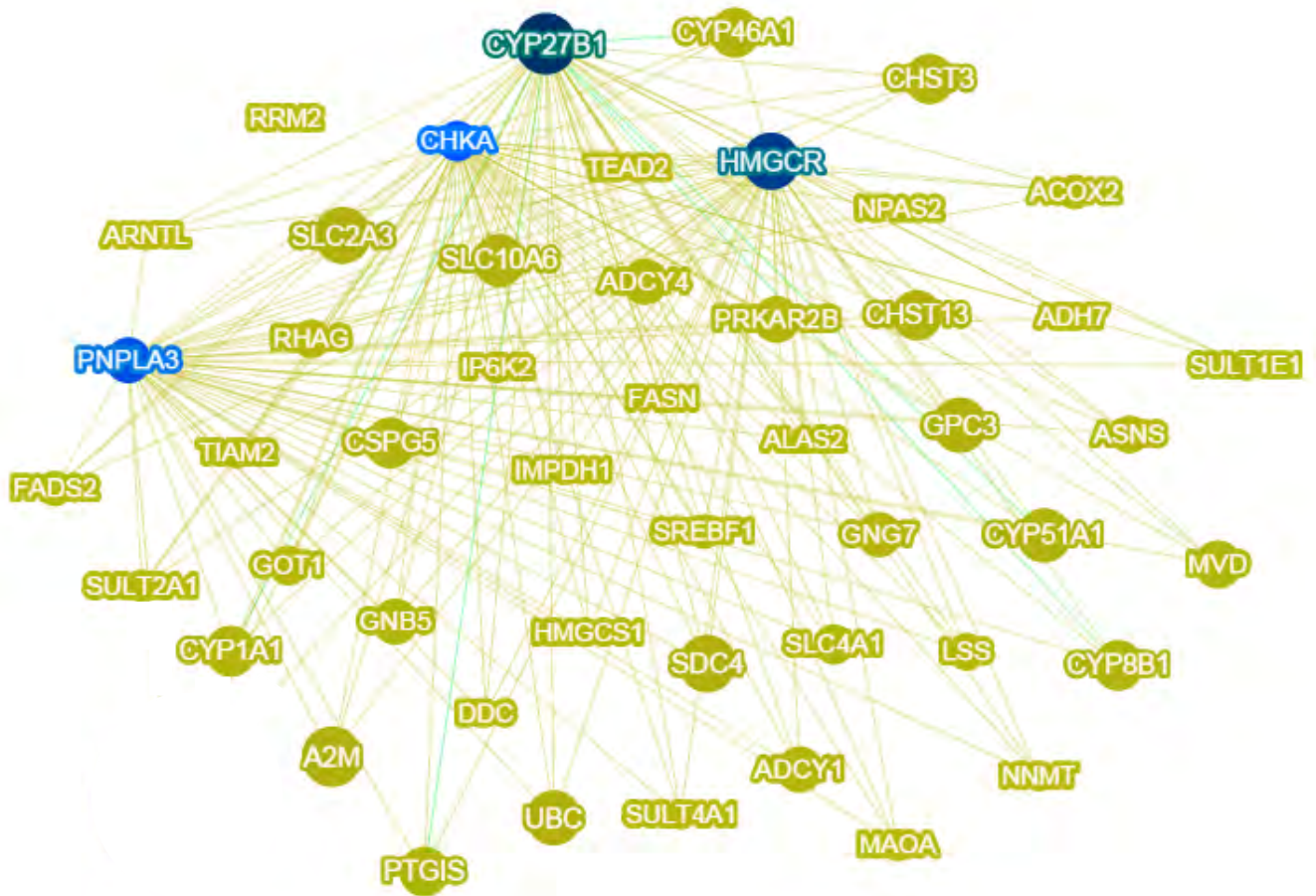
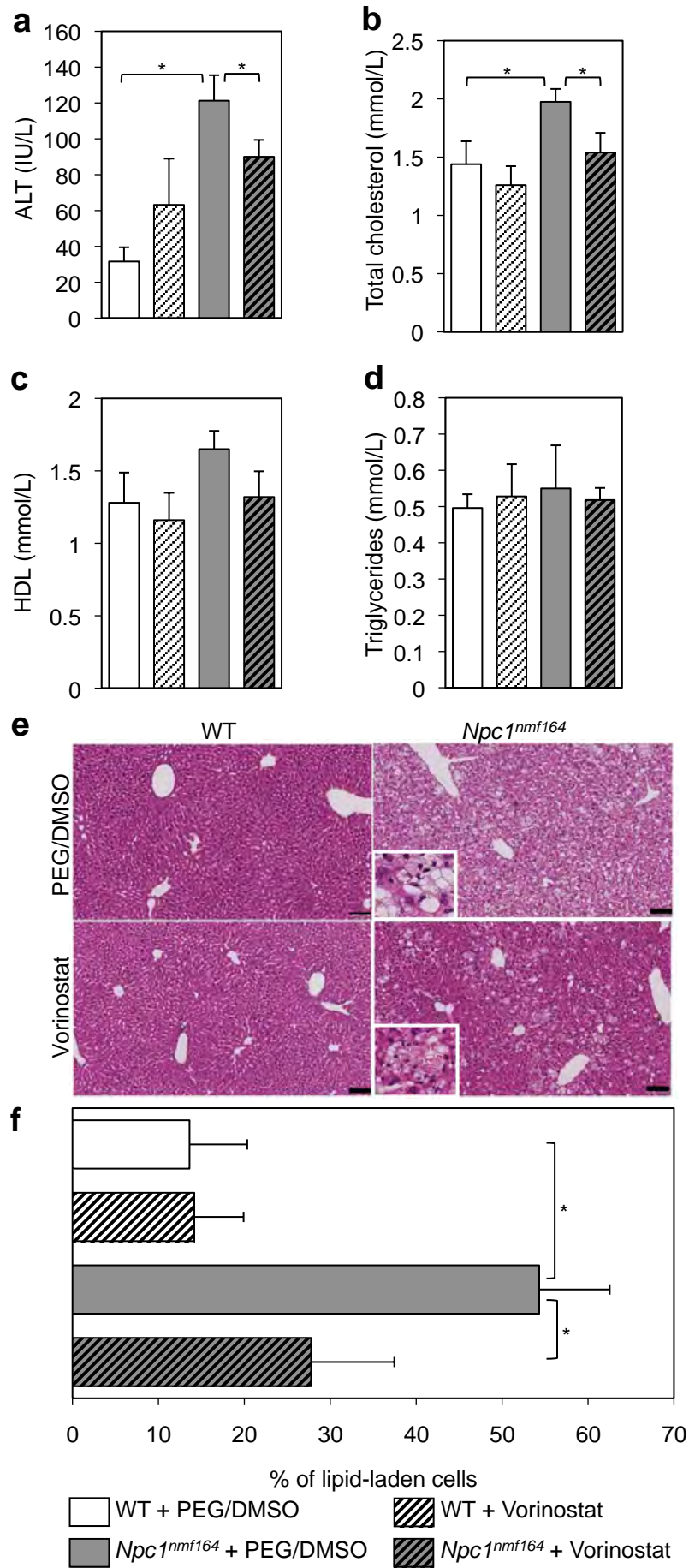


Figure 4





**Figure 5**



**Figure 6**

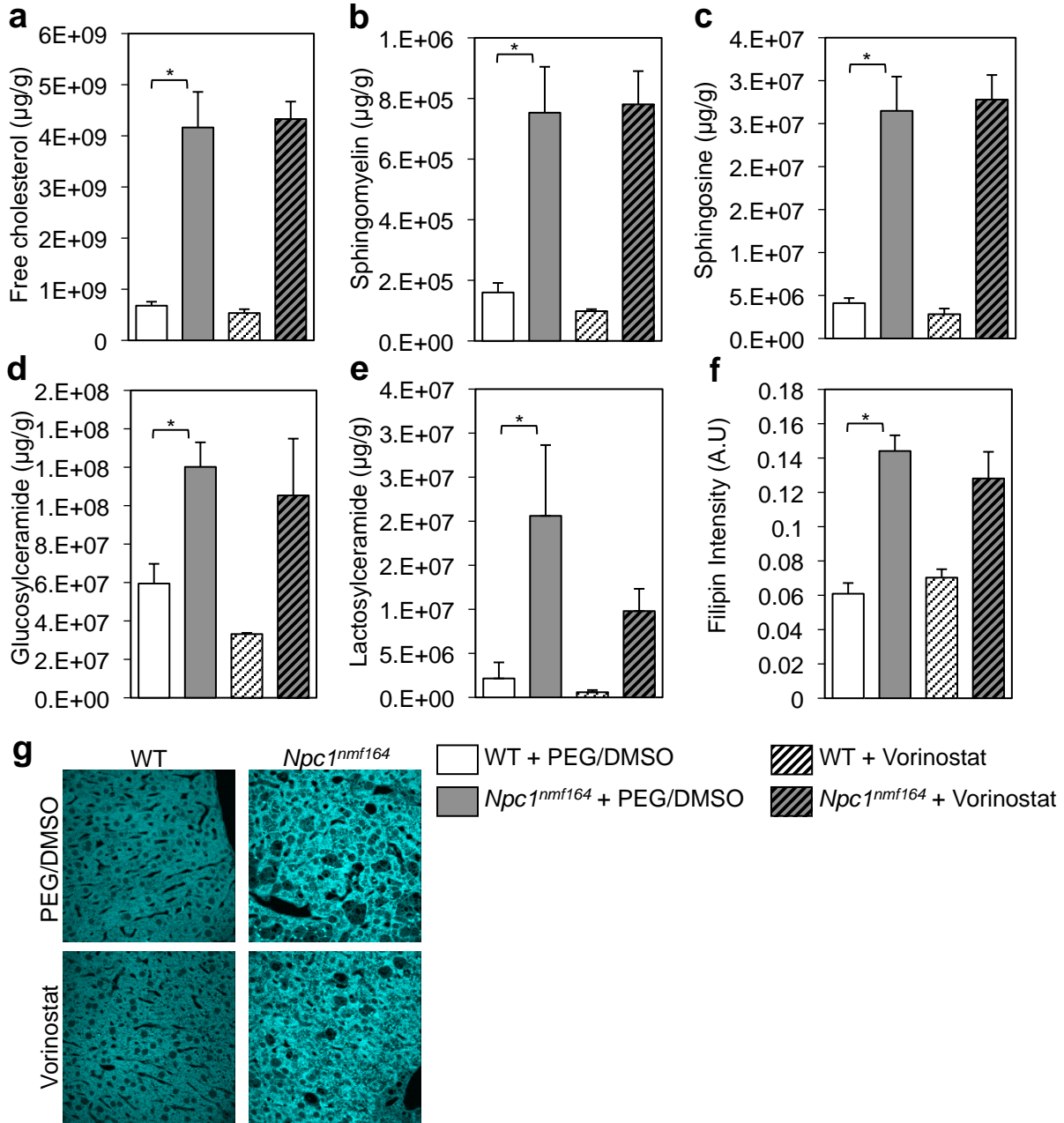


**Figure 7**

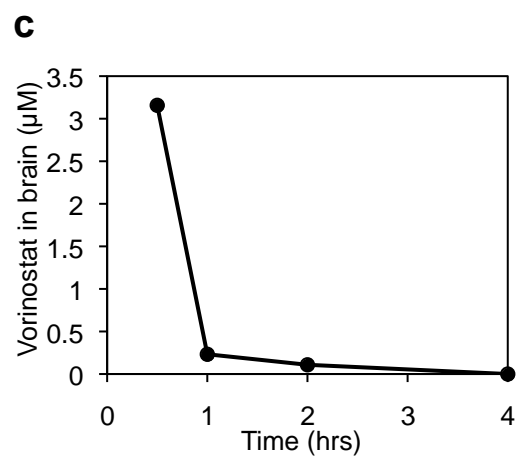
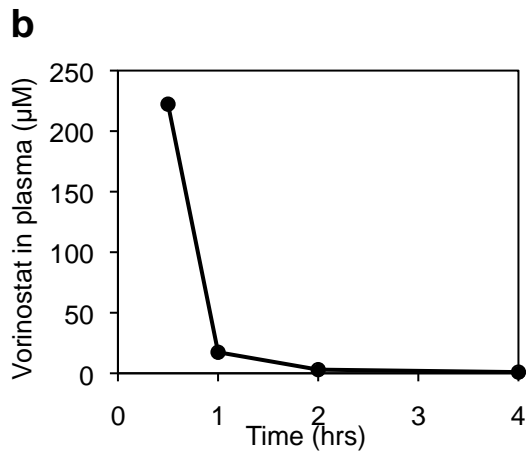
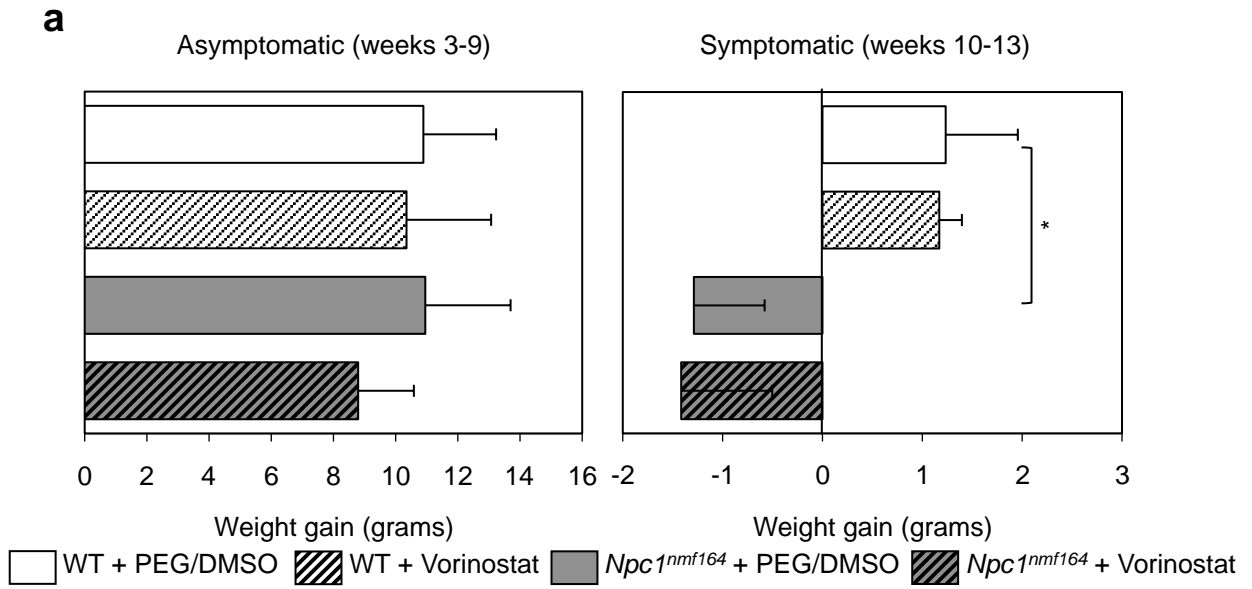


**Figure 8**

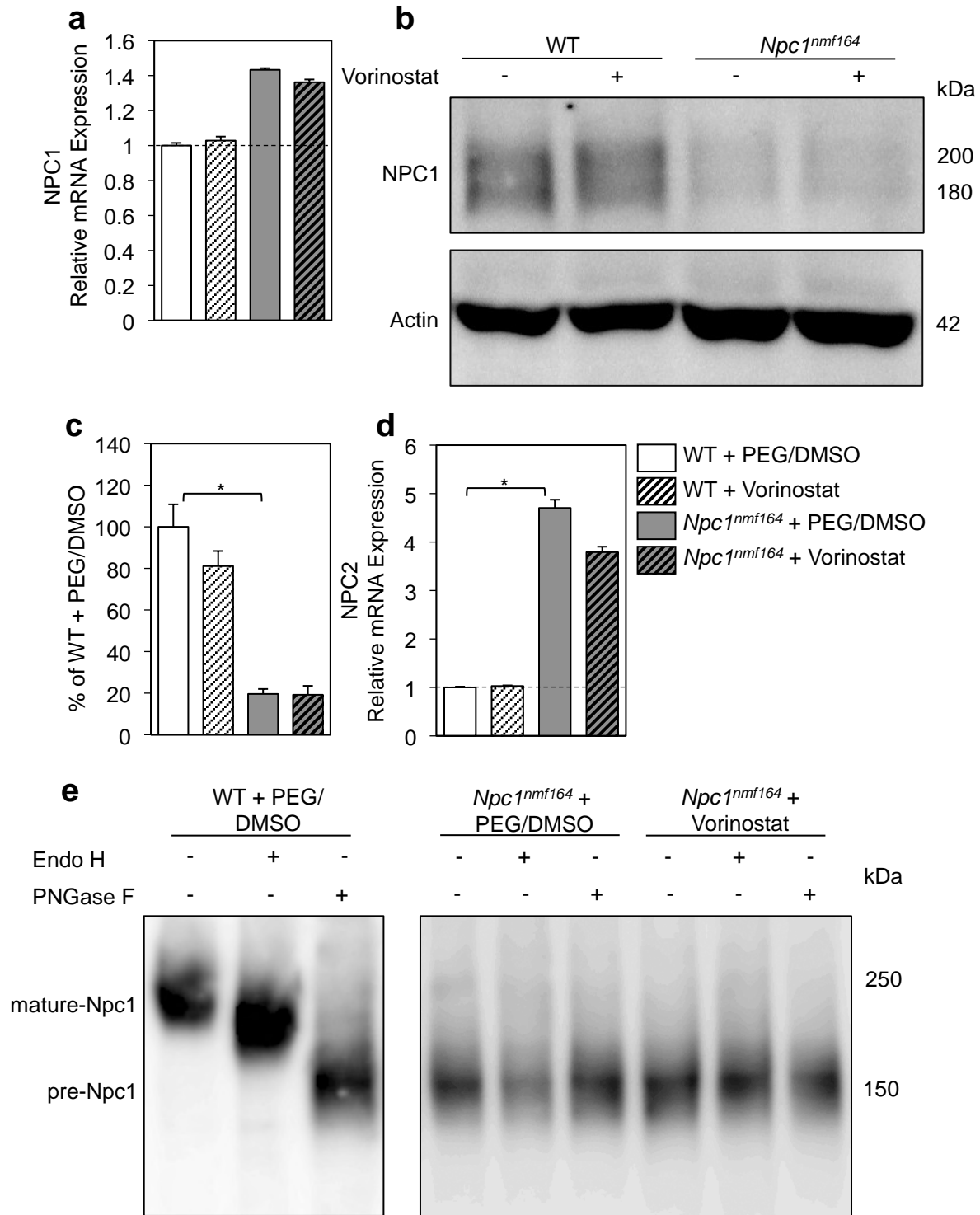


**Figure 9**

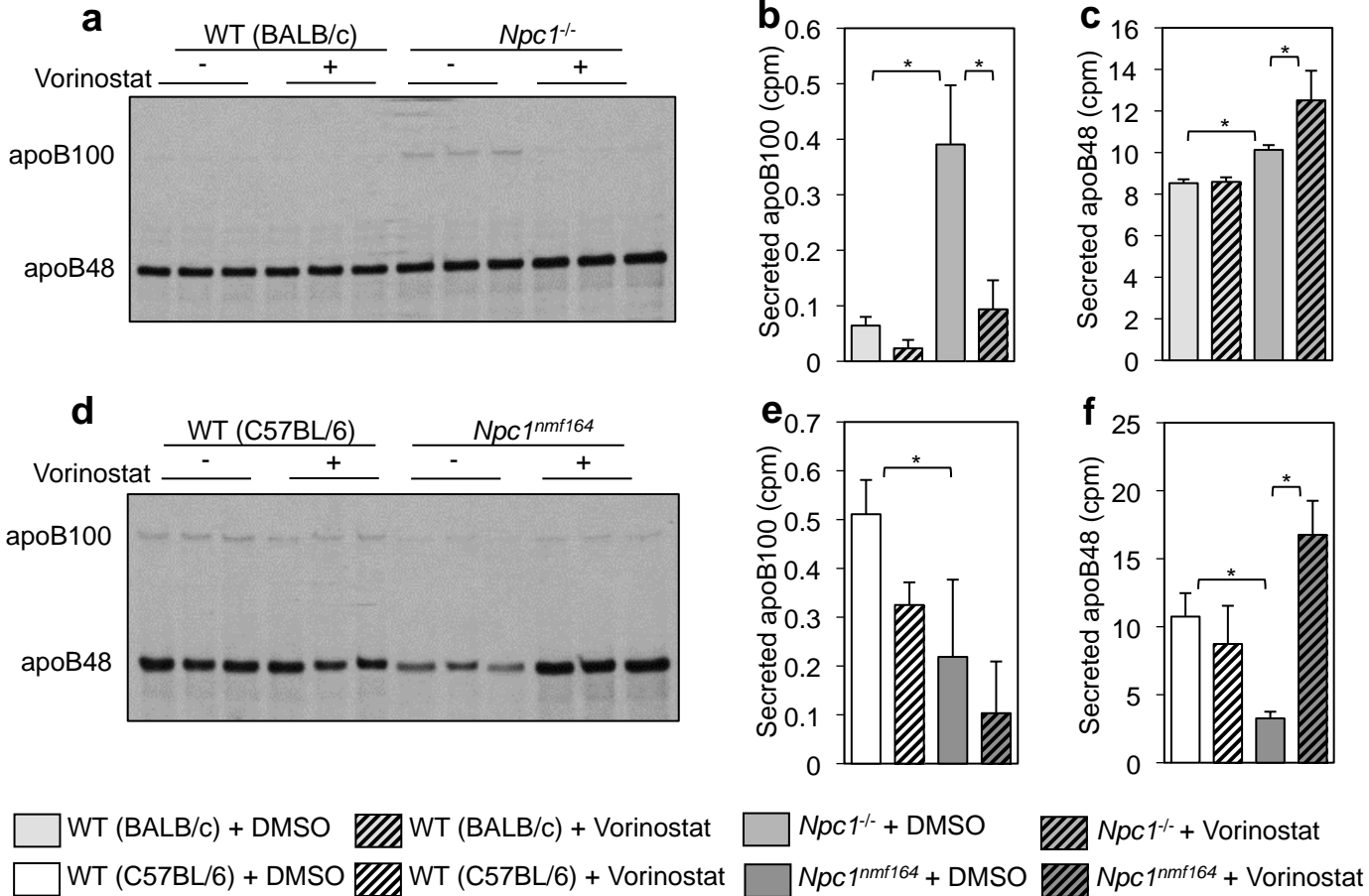
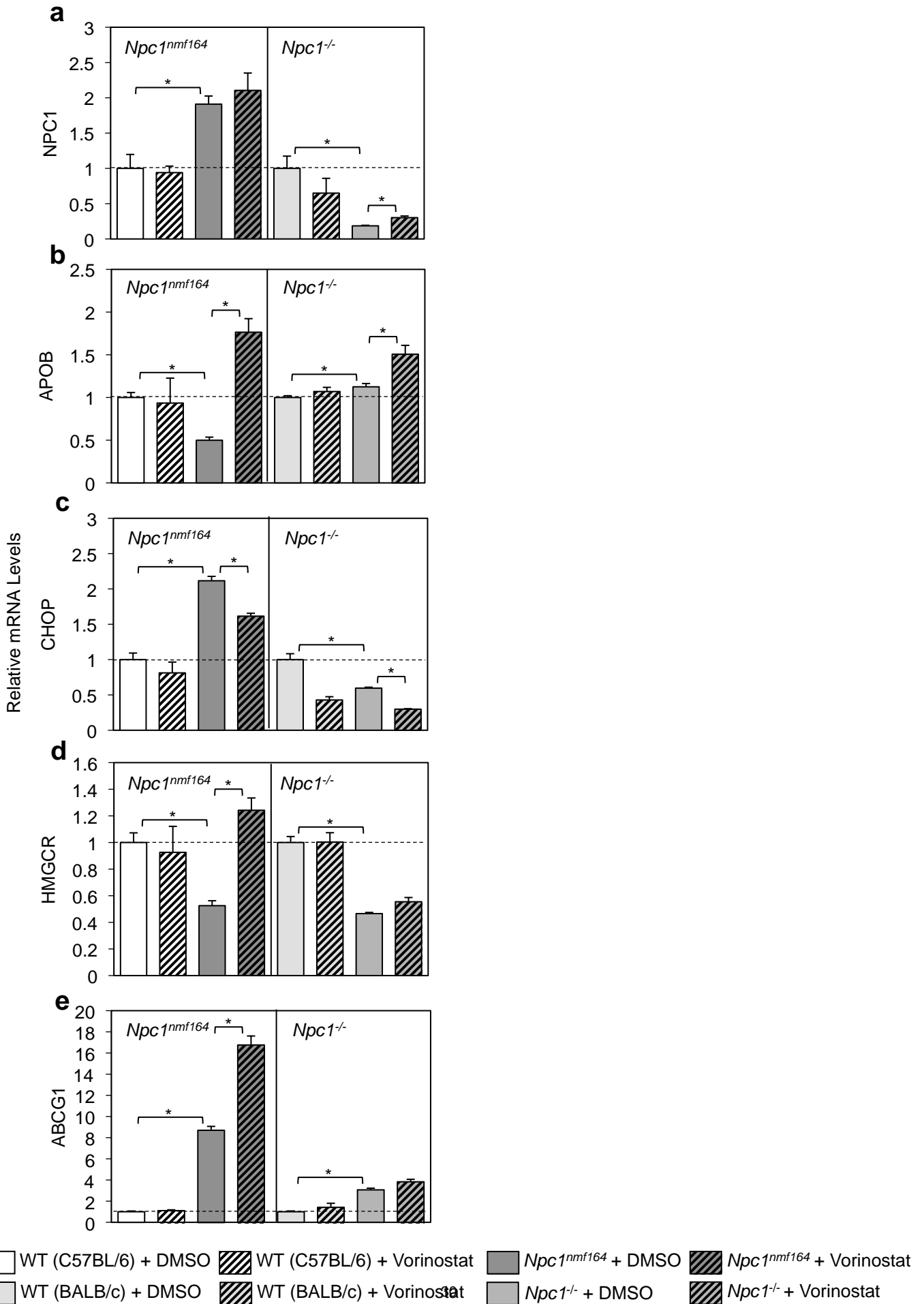


**Figure 10**



**Normalization of Hepatic Homeostasis in the Npc1nmf164 Mouse Model of Niemann-Pick Type C Disease Treated with the Histone Deacetylase Inhibitor Vorinostat**

Andrew B Munkacsi, Natalie Hammond, Remy T Schneider, Dinindu S Senanayake, Katsumi Higaki, Kirill Lagutin, Stephen J Bloor, Daniel S Ory, Robert A Maue, Fannie W Chen, Antonio Hernandez-Ono, Nicole Dahlson, Joyce J. Repa, Henry N. Ginsberg, Yiannis A. Ioannou and Stephen L. Sturley

*J. Biol. Chem.* published online December 28, 2016

---

Access the most updated version of this article at doi: [10.1074/jbc.M116.770578](https://doi.org/10.1074/jbc.M116.770578)

Alerts:

- [When this article is cited](#)
- [When a correction for this article is posted](#)

[Click here](#) to choose from all of JBC's e-mail alerts

This article cites 0 references, 0 of which can be accessed free at <http://www.jbc.org/content/early/2016/12/28/jbc.M116.770578.full.html#ref-list-1>